ANNUAL REVIEWS

Annual Review of Environment and Resources

Insights from Time Series of Atmospheric Carbon Dioxide and Related Tracers

Ralph F. Keeling[1] and Heather D. Graven[2]

[1]Scripps Institution of Oceanography, University of California, San Diego, La Jolla, California 92093, USA; email: rkeeling@ucsd.edu

[2]Department of Physics, Imperial College London, London SW7 2AZ, United Kingdom; email: h.graven@imperial.ac.uk

Annu. Rev. Environ. Resour. 2021. 46:85–110

The *Annual Review of Environment and Resources* is online at environ.annualreviews.org

https://doi.org/10.1146/annurev-environ-012220-125406

Keywords

Mauna Loa record, Keeling Curve, isotope, oxygen, carbonyl sulfide, atmospheric time series

Abstract

The past century has been a time of unparalleled changes in global climate and global biogeochemistry. At the forefront of the study of these changes are regular time-series observations at remote stations of atmospheric CO_2, isotopes of CO_2, and related species, such as O_2 and carbonyl sulfide (COS). These records now span many decades and contain a wide spectrum of signals, from seasonal cycles to long-term trends. These signals are variously related to carbon sources and sinks, rates of photosynthesis and respiration of both land and oceanic ecosystems, and rates of air-sea exchange, providing unique insights into natural biogeochemical cycles and their ongoing changes. This review provides a broad overview of these records, focusing on what they have taught us about large-scale global biogeochemical change.

Contents

1. INTRODUCTION

Sustained measurements of atmospheric CO_2 concentration at remote observatories now span more than 60 years. Measurements of related atmospheric tracers such as the isotopes of CO_2 ($^{14}C/C$, $^{13}C/^{12}C$, and $^{18}O/^{16}O$), atmospheric O_2, and carbonyl sulfide (COS) now also span many decades. Together with records from ice cores, these measurements have assumed a central role in the study of both the causes and consequences of climate change, thus providing critical insights into the functioning of the Earth in a time of rapid global change.

In the 1960s, measurements of rising CO_2 from the Mauna Loa Observatory called attention to the potential threat of anthropogenic climate change and the need for more research (1). This CO_2 record is known as the Keeling Curve after Charles David Keeling, the scientist who initiated and sustained the measurements. Over the years that followed, the continuing CO_2 measurements helped to establish the close relationship between the CO_2 rise and fossil-fuel burning, while also showing that approximately 50% of the excess CO_2 was being removed from the atmosphere by natural processes (2) and that the growth rate fluctuated with El Niño events (3). By the 1980s, a notable increase in the seasonal cycle in CO_2 had been observed, heralding large changes in land ecosystems (4, 5). A major expansion of global measurement networks occurred in the 1980s, led particularly by the US National Oceanic and Atmospheric Administration (6). By the late 1980s, measurements of CO_2, $^{13}CO_2$, and O_2 together confirmed that, along with the oceans, the land biosphere was also a major sink for excess CO_2 (5, 7, 8). A critical early step was the selection of measurement sites to sample background air, which, by virtue of rapid atmospheric mixing, is characteristic of large portions of the atmosphere. The measurements thus provide a holistic perspective on Earth, much like blood pressure and core body temperature provide for human health.

Atmospheric tracer: a chemical compound that is useful as marker for distinct processes, such as atmospheric mixing or exchange with other reservoirs

Background air: air that is free of local influences and thereby characteristic of a large portion of the atmosphere

This article provides an overview of the observed long-term variability in atmospheric CO_2 and the related species, focusing on features that are characteristic of hemispheric or global scales. This article draws on previous reviews on CO_2 growth (9–11), on trends in carbon isotopes of CO_2 (12), and on trends and other variability in atmospheric O_2 and COS (13, 14). We discuss trends, gradients, and cycles in these data, which provide insights into the major processes controlling the buildup of atmospheric CO_2 and the changing biogeochemistry of the land and oceans. Many of these records touch on related topics, such as the strength of land and ocean carbon sinks,

the sensitivity of carbon exchange to climate changes, and the detection of large-scale metabolic changes. For each species, we describe the basic biogeochemical controls, provide a brief historical context, and review recent literature to highlight major discoveries. In the final section, we summarize major insights and opportunities going forward, including the continuing relevance of these measurements to studies of the carbon cycle in the context of global climate change.

2. VARIATIONS IN ATMOSPHERIC CO_2

2.1. Global Trend in CO_2

Atmospheric CO_2 concentration has been directly measured since the late 1950s at a growing number of stations around the world (15, 16). Measurements of old air preserved in Antarctic ice cores have allowed atmospheric CO_2 concentration to be determined for earlier periods, although with more limited temporal resolution (17, 18). These measurements (**Figures 1** and **2**) document an accelerating growth in atmospheric CO_2 that began around 1800 from a natural preindustrial level of approximately 280 ppm, which prevailed with only small deviations (~10 ppm) over the previous 10,000 years of the Holocene (18). Atmospheric CO_2 concentration at Mauna Loa, Hawaii, was 414 ppm in 2020, nearly 50% higher than the preindustrial concentration. The measurements also show variability on seasonal, interannual, and decadal timescales, which we discuss below.

The atmosphere is sufficiently well mixed on timescales of a few years or more (19) that the trend in CO_2 can be understood on the basis of global mass balance. The trend is driven by CO_2 sources from fossil-fuel burning (*FF*) and land use (*LU*), which are partially offset by sinks from the ocean (O) and land biosphere (B):

$$M \cdot \mathrm{d}C_a/\mathrm{dt} = FF + LU - O - B, \qquad 1.$$

where $\mathrm{d}C_a/\mathrm{dt}$ is the trend in CO_2 in ppm, M is a conversion factor of 2.12 Pg C ppm^{-1}, and all other terms are in units of Pg C/year. *FF* includes a small contribution from cement manufacture.

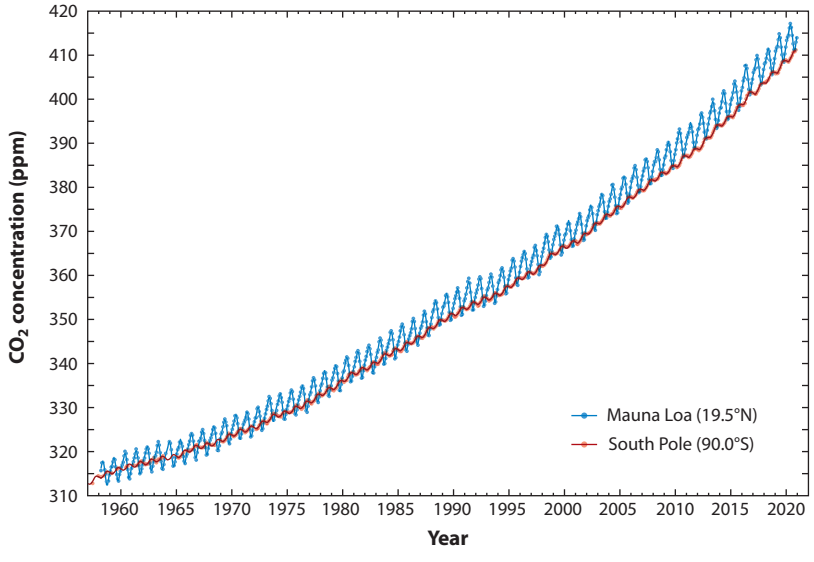

Figure 1

Monthly CO_2 concentrations measured at Mauna Loa, Hawaii (19.5°N) and South Pole (90.0°S) observatories by the Scripps CO_2 program (**https://scrippsco2.ucsd.edu**).

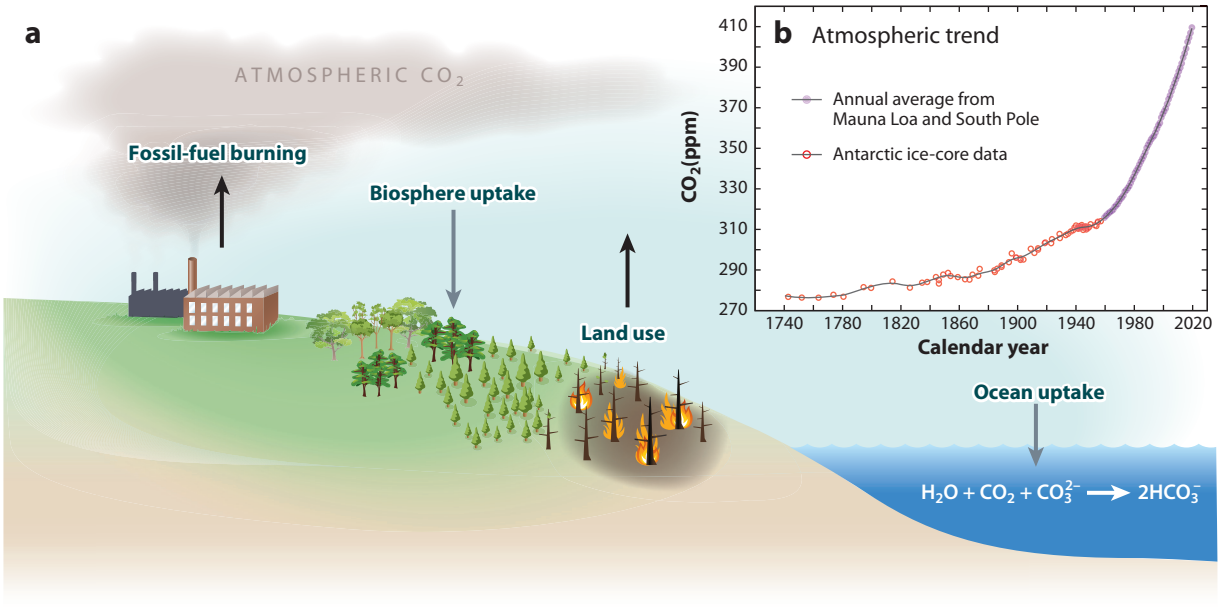

Figure 2

(*a*) Diagram of the main controls on the atmospheric CO_2 rise, showing sources from fossil-fuel burning and land use and the sinks in the land biosphere and ocean, which partly buffer the rise. (*b*) Time series of CO_2 concentration, estimated from the average of the Mauna Loa and South Pole annual means (*purple solid dots*) and from Antarctic ice-core data (*red open circles* and *spline fit*) (17).

Airborne fraction: the ratio of the rise in atmospheric CO_2 to the emissions over a particular time frame (e.g., annually)

The ocean and land sinks are sometimes called natural sinks because they reflect natural processes that buffer the atmospheric CO_2 rise, such as carbonate chemistry in seawater and photosynthetic uptake of CO_2 by land ecosystems. However, although the underlying processes are natural, the sinks result from human-induced imbalances to the carbon cycle that did not previously exist.

Estimates of the terms in Equation 1 have been compiled by the Global Carbon Project (10) on an annual basis. **Table 1** shows results for the decade 2010–2019. The atmospheric growth term is derived from global observations, similar to **Figure 1**. Fossil-fuel and cement emissions are derived from industrial records. Land-use emissions conceptually include contributions from deforestation, afforestation, logging, forest degradation, shifting cultivation, etc., and are estimated by combining historical records of land use with estimates of carbon densities.

The atmospheric rise accounts for 46% of total emissions (*FF* + *LU*) or 54% of fossil-fuel emissions (*FF*) over 2010–2019 (**Table 1**). This rise/emission ratio, known as the airborne fraction, has remained relatively constant since 1960 (9, 20), showing that the land and ocean sinks have

Table 1 The global carbon budget for January 2010–December 2019 from Friedlingstein et al. (10)

Term	Magnitude (Pg C/year)	Fraction of total emissions (*FF* + *LU*)	Fraction of fossil-fuel emissions (*FF*)
Fossil fuel and cement (*FF*)	9.4 ± 0.5	85%	100%
Land use (*LU*)	1.6 ± 0.7	15%	17%
Atmospheric increase ($M \cdot dC_a/dt$)	5.1 ± 0.2	46%	54%
Land biosphere sink (*B*)	3.4 ± 0.9	23%	36%
Ocean sink (*O*)	2.5 ± 0.6	27%	26%

grown roughly proportionally with emissions. The detection of long-term changes in the airborne fraction (using $FF + LU$) is limited by uncertainty in land-use emissions (21).

The ocean sink term in **Table 1** is based on an ensemble of ocean models that simulate the chemistry of CO_2 in seawater and rates of ocean mixing. The ocean sink can also be estimated from a range of observational methods (10), including trends in atmospheric O_2, as discussed below. These alternate estimates of the ocean sink are in relatively good agreement.

The global land sink term merits special attention. The estimate in **Table 1** of 3.4 ± 0.9 Pg C/year uses the mean and standard deviation of an ensemble of dynamic global vegetation models. From a modeling standpoint, however, unlike the ocean sink, the processes controlling the land sink are still imperfectly understood, and different models disagree (22, 23). There is a consensus that the sink is at least partly accounted for by CO_2 fertilization, but the magnitude of this effect is still highly uncertain [±100% (22)], and the relative role of other processes such as climate impacts on land ecosystems and the role of anthropogenic nitrogen inputs is unclear (24). The model ensemble standard deviation of ±0.9 Pg C/year (or ±26%) therefore cannot reflect the full process-level uncertainty, which is much larger. The model mean is very similar to the residual sink of 3.5 ± 1.1. Pg C/year that is required to balance the budget (residual sink = $FF + LU - M \cdot dC_a/dt - O$), which likely reflects some degree of tuning of the land models to balance the global budget.

2.2. Seasonal Cycles in CO_2

Throughout the Northern Hemisphere, atmospheric CO_2 undergoes a regular seasonal cycle with a peak in late spring and a trough in late summer or early fall. This cycle was first discovered in 1960 and recognized as a signal of seasonal uptake and release of CO_2 from the land biosphere in the Northern Hemisphere (25), which has been confirmed by modeling studies and isotopic measurements (26). The amplitude is weaker, and the phasing is later at lower latitudes compared to higher latitudes (**Figure 3**). In the Southern Hemisphere, a much weaker cycle is found, as expected from the smaller land area.

Intriguingly, the amplitude of the cycle in the Northern Hemisphere has increased markedly since the 1960s, with the phasing of the summer drawdown shifting earlier by ~1 week. **Figure 3** shows the longest records from Barrow (71°N) and Mauna Loa (20°N). The increase was already evident in the 1980s (27, 28) and has continued to the present, superimposed on interannual variability (29–31). Measurements made by aircraft and at surface stations show that the amplitude increase is much larger north of 45°N (31, 32). Due to atmospheric mixing, the changes in CO_2 amplitude seen in any given location depend on changes in CO_2 flux over a wide portion of the Northern Hemisphere.

Despite the clear evidence for changes in seasonal amplitude, a firm mechanistic understanding of the cause is still lacking. The observed pattern indicates that CO_2 uptake in the spring/summer growing season has increased over large areas of boreal, Arctic, and temperate ecosystems, potentially focused in Eurasia (31–33). Simulations with biogeochemical models driven by CO_2 changes, climate changes, and land-use changes over the past decades typically show amplitude increases but disagree on the relative importance of the different driving mechanisms and underestimate the observed trends (31, 34). The most consistent factor across models tends to be CO_2 fertilization, but they disagree on the magnitude of this effect and the impact of other factors such as climate change and land use. The most recent models suggest that changes in cropland area have played at most a minor role in the amplitude changes north of 45°N (34). One hypothesis is that photosynthesis per unit of light absorbed may have risen more than in the models (34), which is consistent with other observations including increases in leaf area measured by satellite and increases in global gross primary production (GPP) based on COS (35).

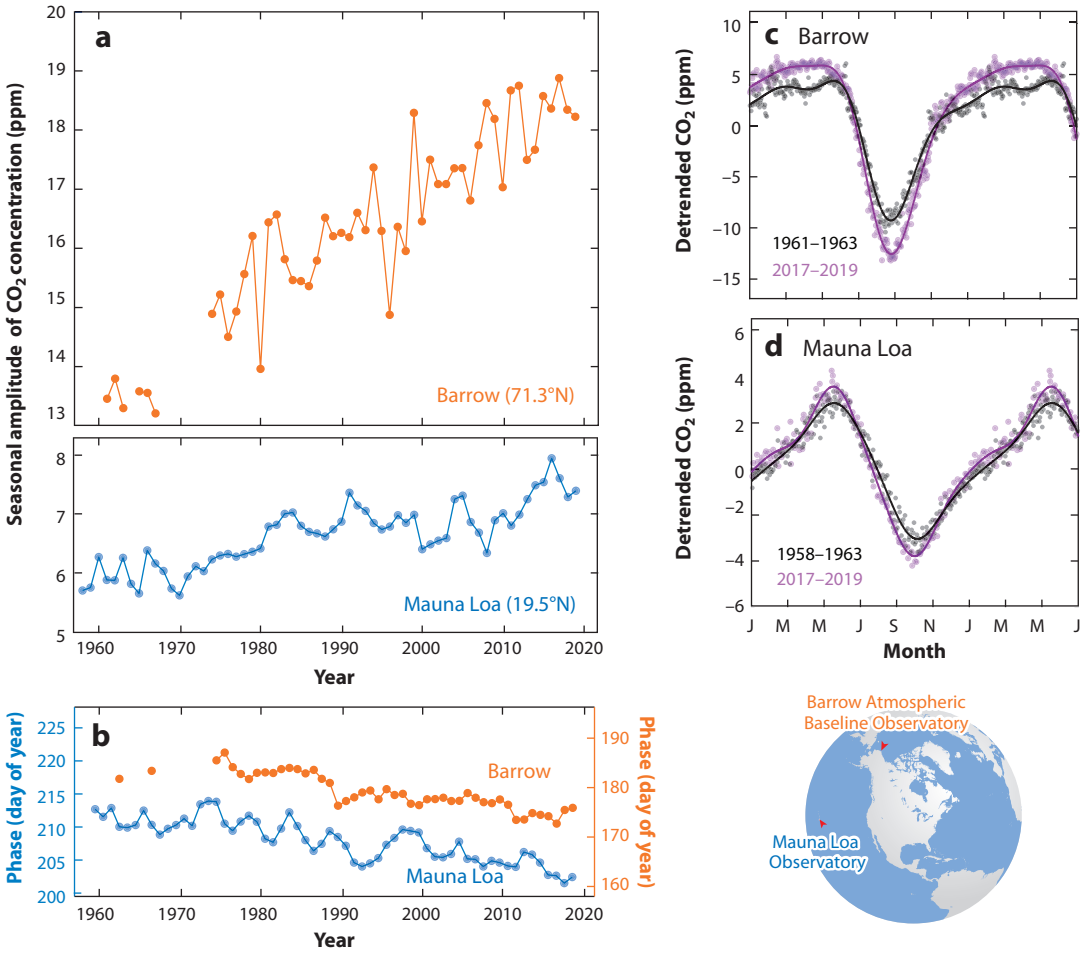

Figure 3

Observed peak-to-trough of (*a*) amplitude and (*b*) phase based on day of year of downward zero crossing of CO_2 at Barrow, Alaska (71.3°N, *orange dots*, *right axis*) and Mauna Loa, Hawaii (19.5°N, *blue dots*, *left axis*) as measured by the Scripps CO_2 program and the National Oceanic and Atmospheric Administration Global Monitoring Division. Seasonal cycles at (*c*) Barrow and (*d*) Mauna Loa for the periods indicated. Data were interannually detrended to center on zero when computing cycles. Adapted from 31 with permission from the AAAS.

An important role may be played by warming trends in spring months, which allow plants to become active earlier in the season and may enhance growing-season productivity (29, 36). More generally, a strong link to warming is suggested by the larger amplification of the CO_2 cycle at higher latitudes, where warming has occurred more rapidly (32). Another significant change in the cycle is the earlier shift of the upwards zero crossing, suggesting increases in fall respiration are also occurring, possibly linked to warming (37).

2.3. Variations on El Niño and Interannual Timescales

The annual growth rate of CO_2 exhibits significant variability on interannual timescales (**Figure 4**). These fluctuations are much too large to be caused by year-to-year variations in fossil-fuel emissions. High growth rates tend to occur during and following El Niño years, when

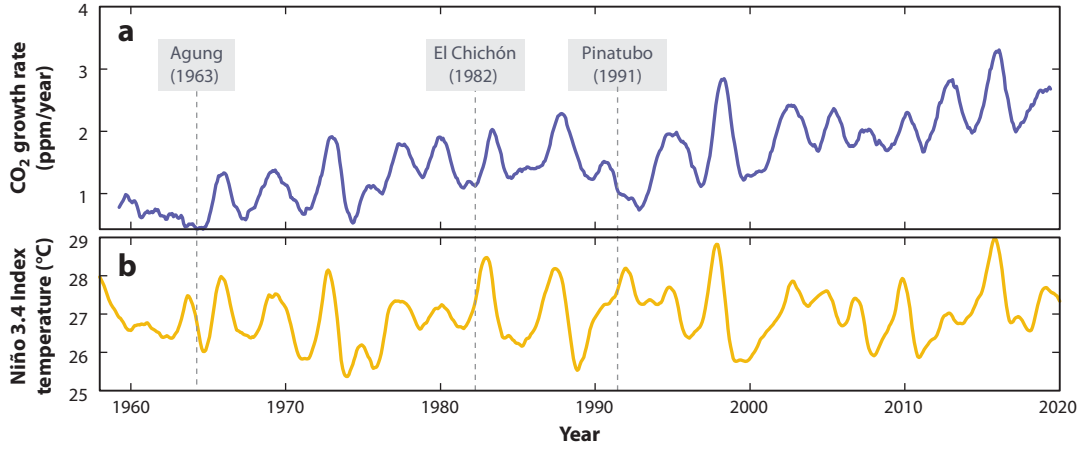

Figure 4

(*a*) Time derivative of the CO_2 growth rate calculated from average of records at Mauna Loa, Hawaii (19.5°N) and the South Pole (90.0°S). (*b*) Annual running mean temperature of the National Centers for Environmental Prediction Niño 3.4 Index, which is an index used to define El Niño events based on sea-surface temperatures in a region of the Eastern Tropical Pacific Ocean (**https://psl.noaa.gov/data/correlation/nina34.data**). The CO_2 time derivative was computed from one-year differences of running annual mean at monthly resolution. Also shown is the timing of major volcanic eruptions (*gray boxes*).

sea-surface temperatures along the Equator in the Eastern Tropical Pacific are anomalously warm. Low growth rates accompany the counterpart La Niña years. This link to El Niño events was first noted by Bacastow (3), who assumed the fluctuations were of oceanic origin. In fact, this phenomenon was later shown to be caused primarily by natural fluctuations of the tropical land biosphere, based on isotopic measurements (38, 39) and inverse modeling (40). During El Niño years, warm and dry conditions prevail over much of the tropical land masses, decreasing photosynthetic CO_2 uptake and increasing CO_2 release by respiration and fire. The oceans play a much weaker and partly counteracting role, as reduced upwelling during El Niño events restricts the natural outgassing of CO_2 in the Eastern Equatorial Pacific (41, 42). Recent work indicates that the CO_2 fluctuations may originate from not just tropical forests but also semiarid tropical ecosystems, such as savannas (43, 44).

The interannual CO_2 fluctuations provide an important test for our understanding of the response of tropical ecosystems to short-term climate fluctuations. For example, Cox et al. (45) showed that the predicted impact of global warming on Amazonian rain forests correlated with the strength of the modeled El Niño CO_2 signal, allowing future responses to be narrowed by rejecting models with unrealistic El Niño signals. An important mechanistic question concerns the roles of temperature and moisture. Tropical drought, as measured by soil moisture, tends to cause reductions in both photosynthesis and respiration, with a larger impact on photosynthesis, whereas warm anomalies tend to suppress photosynthesis but enhance respiration (46). Temperature and hydrological changes during El Niño conditions thus both lead to anomalous CO_2 release. A strong role for hydrological changes in driving the interannual CO_2 fluctuations is indicated by strong correlations with satellite-determined terrestrial water storage (47), which is consistent with the large drought effect found in local studies (43, 44). Temperature effects are clearly also important at the global scale (46). The growth rate of CO_2 was anomalously low after the major volcanic eruptions of Agung in 1964, El Chichón in 1982, and Pinatubo in 1991 (41). This response has been attributed primarily to reduced soil respiration caused by cooling, although other causes also have been considered (48, 49).

Additional variability in CO_2 growth that is not tied to fossil-fuel burning or volcanos is also detectable on decadal timescales, such as slower than expected growth in the 1940s and 2000s (50, 51). These longer-term perturbations may be partly explained via tropical processes similar to the El Niño response but projected onto longer timescales (20).

2.4. Interhemispheric CO_2 Gradient

The atmospheric CO_2 records show a growing CO_2 excess in the Northern Hemisphere compared to the Southern Hemisphere (**Figure 1**). The difference between annual CO_2 levels at Mauna Loa and the South Pole, for example, has grown from ~0.5 ppm in 1960 to ~4 ppm in the 2010s.

The main process accounting for this north–south gradient is the burning of fossil fuels, which occurs mostly in the Northern Hemisphere. Intriguingly, a plot of the CO_2 gradient versus global fossil-fuel emissions (**Figure 5**) yields nearly a straight line with an intercept of –0.6 ppm and a slope of 0.45 ppm/Pg C year^{-1}. This linear relationship is a striking emergent property of the carbon system (52). If fossil-fuel burning were the only influence on the gradient, an intercept of zero and slope of >0.60 ppm/Pg C year^{-1} would be expected (53). The negative intercept could have several causes (52, 54) but is best explained by natural processes (e.g., horizontal transport of carbon in oceans and rivers), which, in the absence of human carbon sources and sinks, produce a slight excess of CO_2 in the Southern Hemisphere (55).

The lower-than-expected slope must arise from the impacts of the land and ocean carbon sinks. The ocean sink, however, acts to increase, not decrease, the gradient. This is because more anthropogenic CO_2 is taken up by the ocean in the Southern than Northern Hemisphere (54). The land sink must therefore more than offset the growing impact of the ocean sink on the gradient. Tropical ecosystems can have little impact on the gradient because their impact

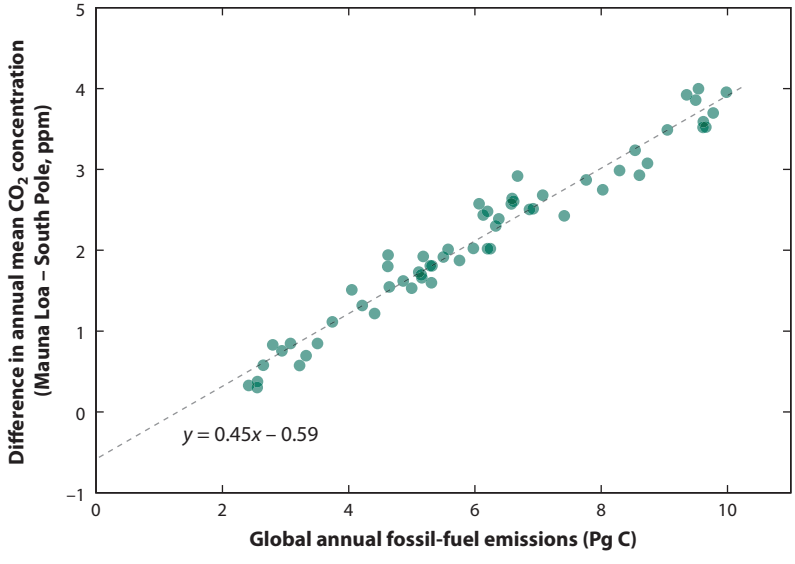

Figure 5

Difference in annual-mean CO_2 concentration between Mauna Loa, Hawaii (19.5°N) and South Pole (90.0°S) observatories (*y*-axis) versus global fossil-fuel emissions (*x*-axis). Based on annual means for each calendar year. Dashed line is linear least-squares fit.

on atmospheric CO_2 is spread symmetrically between the hemispheres (52). Ecosystems in the southern extratropics also cannot be important because of their small land area. The lower-than-expected slope therefore requires a land sink in the northern extratropics. The existence of a northern land sink was first highlighted in the landmark studies of the interhemispheric gradient by Tans et al. (7) and Keeling et al. (56), which helped to cement the major role of the land biosphere as a CO_2 sink. Like the constant airborne fraction, the growing atmospheric CO_2 gradient and constant slope indicate the land and ocean sinks have continued to grow in proportion to fossil-fuel burning over the past 50 years (53, 54).

3. VARIATIONS IN CARBON ISOTOPES OF CO_2

3.1. Radiocarbon

A very small fraction ($\sim 10^{-12}$) of the carbon in atmospheric CO_2 is comprised of the radioactive isotope ^{14}C, also known as radiocarbon. ^{14}C is naturally produced in the upper atmosphere by cosmic rays via neutron capture by nitrogen and artificially produced by nuclear weapons testing and to a small degree by nuclear reactors (**Figure 6**). With a half-life of 5,700 years, ^{14}C can readily spread from the atmosphere into the oceans and the land biosphere before decaying. Carbon reservoirs that were recently sourced from the atmosphere, such as leaves, will have a $^{14}C/C$ ratio similar to atmospheric CO_2, whereas reservoirs that are more isolated (such as the deep ocean) will have lower $^{14}C/C$ ratios due to radioactive decay. The natural abundance of ^{14}C in atmospheric CO_2 reflects a quasi-steady-state balance between production by cosmic rays and loss by decay and dispersal into the other reservoirs.

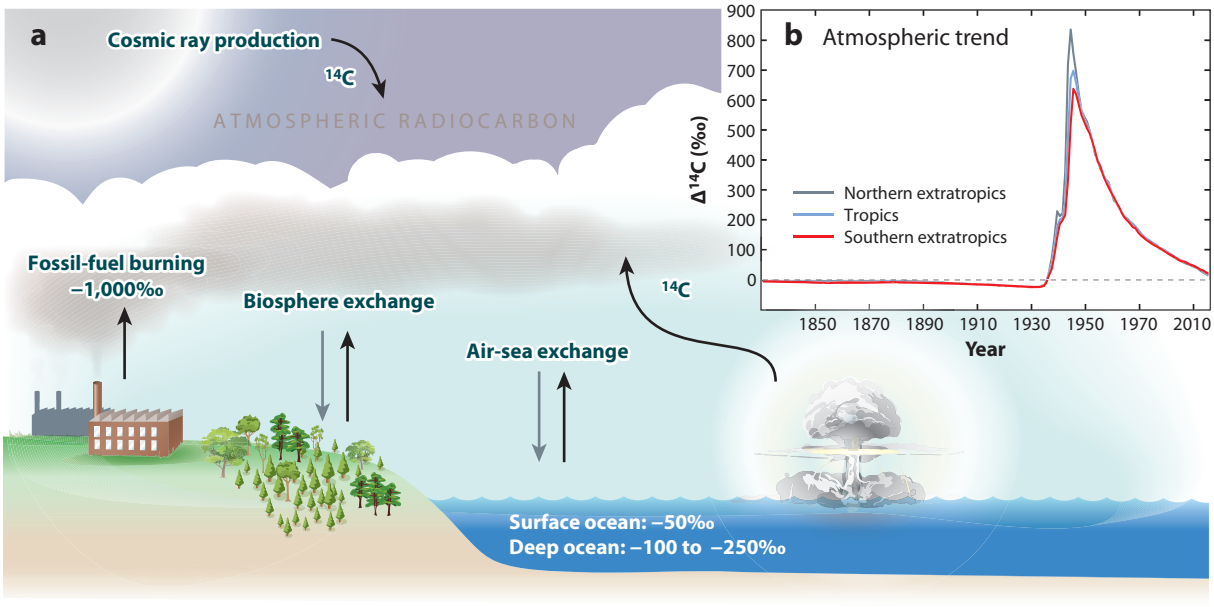

Figure 6

(*a*) Diagram of main controls on atmospheric radiocarbon, showing preindustrial ranges of $\Delta^{14}C$ in land biospheric and oceanic reservoirs. (*b*) Annual-mean $\Delta^{14}C$ values for three zonal bands representing the northern extratropics (30–90°N), tropics (30°S–30°N), and southern extratropics (30°–90°S), as presented in Graven et al. (12, 61).

Suess effect: the decrease in the $^{14}C/C$ ratio of atmospheric CO_2 caused by the input of ^{14}C-free CO_2 from fossil-fuel burning

Atmospheric radiocarbon measurements are conventionally reported in $\Delta^{14}C$ notation in permil, reflecting deviations in $^{14}C/C$ from a standard ratio. $\Delta^{14}C$ is notionally equal to $(r_{sample} - r_{standard})/r_{standard} \times 1{,}000$, where r is the $^{14}C/C$ ratio, but it includes small corrections for sample age and $^{13}C/^{12}C$ ratio. The primary standard is based on samples of oxalic acid and defined to be similar to atmospheric $\Delta^{14}C$ in 1890 (57).

Direct measurements of atmospheric $\Delta^{14}C$ began in the 1950s and continue at a limited number of sites today (58–62). Although ice cores are problematic for radiocarbon because of cosmic ray production of ^{14}C within polar ice (63), earlier $\Delta^{14}C$ variations can be reconstructed from reservoirs that were directly sourced from atmospheric CO_2 and can be independently dated, such as tree rings or varved lake sediments (64). **Figure 6** shows compiled records of $\Delta^{14}C$ since 1850.

The most prominent perturbation to atmospheric $\Delta^{14}C$ of the past century is the spike caused by atmospheric testing of nuclear weapons (58), which produced excess ^{14}C via neutron reactions, similar to cosmic ray production (**Figure 6**). By the time of the Partial Test Ban Treaty in 1963, the radiocarbon content of the atmosphere had nearly doubled, increasing to ~835‰ in the Northern Hemisphere and 635‰ in the Southern Hemisphere (60). In the following decades, this bomb spike mostly dissipated, as the excess ^{14}C spread from the atmosphere into the ocean and land biosphere carbon reservoirs, with the dissipation rate controlled by CO_2 exchange with and within these reservoirs.

Another major perturbation has been fossil-fuel burning. Fossil fuels are devoid of ^{14}C, corresponding to $\Delta^{14}C = -1{,}000‰$ ($r_{sample} = 0$). The addition of fossil-fuel CO_2 to the atmosphere therefore decreases $\Delta^{14}C$ while increasing atmosphere CO_2. Before the onset of the bomb tests, fossil-fuel CO_2 emissions caused $\Delta^{14}C$ to drop from a preindustrial value near zero to –20‰. The detection of this decrease in tree rings by Hans Suess (65) comprised the first evidence of a human imprint on atmospheric CO_2. In honor of this important discovery, the fossil-fuel impact on atmospheric $\Delta^{14}C$ is known as the Suess effect. During the first few decades after the bomb tests, the Suess effect was dwarfed by the bomb perturbation. In recent decades, however, as the bomb spike has mostly dissipated, the main driver of the decreasing $\Delta^{14}C$ trend is again the Suess effect (60, 66) and $\Delta^{14}C$ will soon drop again below the 0‰ preindustrial level (12).

Measurements of atmospheric $\Delta^{14}C$ at background air stations also show variations on shorter timescales. In the early 1960s, $\Delta^{14}C$ underwent marked seasonal variations of approximately 50‰ due to the seasonality in the exchange of air between the troposphere and stratosphere, where the bomb ^{14}C was initially injected (59). More recently, seasonal cycles of 3 to 10‰ are evident, depending on station location, which partly reflect continuing seasonal injection of natural cosmic ray–produced ^{14}C from the stratosphere (60, 67). Stratospheric inputs may also explain small variations evident on multi-year timescales that correlate with the quasi-biennial oscillation (66). A substantial interhemispheric gradient with excess ^{14}C in the north was evident in the 1960s, as the bomb testing was mostly done in the Northern Hemisphere. In recent years, the north–south $\Delta^{14}C$ gradient has reversed sign owing to the strong impact of fossil-fuel burning concentrated in the Northern Hemisphere, but with counteracting influences on the gradient from the oceans and the land biosphere (60, 67).

Measurements of atmospheric ^{14}C, when combined with ^{14}C measurements in the ocean and the land biosphere, have been applied to address a wide range of geochemical questions. Measurements of $\Delta^{14}C$ in the ocean have quantified the uptake of bomb ^{14}C by the ocean (68, 69). Together with the atmospheric data, these measurements quantify the air-sea gas exchange velocity, which dictates the rate the upper ocean equilibrates with atmospheric CO_2 (69–71). The data have also historically played a key role in quantifying the global ocean carbon sink (68). Via mass balance

(72), the combined ocean and atmospheric datasets yield estimates of the uptake of bomb ^{14}C by the land biosphere, which provides constraints on global rates of photosynthetic net primary production of the land biosphere (60, 73). The ^{14}C-based constraints on air-sea and atmospheric-biosphere exchange improve our understanding of the controls on atmospheric ^{13}C, thus enabling more powerful ^{13}C applications (73, 74). $\Delta^{14}C$ measurements are also being developed to quantify CO_2 emissions from fossil-fuel burning, which are devoid of ^{14}C. This application is difficult at the global scale due to uncertainty in other influences on $\Delta^{14}C$ (60), but it is very promising at continental or smaller scales, including urban environments (75–77).

Disequilibrium flux: exchange of isotopes at the interface between two reservoirs, driven by the reservoirs being out of isotopic equilibrium and not necessarily associated with any carbon loss or gain

^{13}C-Suess effect: the decrease in the $^{13}C/^{12}C$ ratio of atmospheric CO_2 caused by the input of ^{13}C-depleted CO_2 from fossil-fuel burning

3.2. Carbon-13

Carbon has two stable isotopes, ^{12}C and ^{13}C, with roughly 99% present as ^{12}C and 1% as ^{13}C. Variations in the $^{13}C/^{12}C$ ratio are typically small, but they can provide useful information. One source of variability is photosynthesis, which involves isotopic discrimination via selective uptake of $^{12}CO_2$ relative to $^{13}CO_2$, producing biomatter that is approximately 2% depleted in ^{13}C relative to the ratio in the air and leaving behind CO_2 in the air that is enriched in ^{13}C (i.e., higher $^{13}C/^{12}C$ ratio). Photosynthesis therefore increases the $^{13}C/^{12}C$ ratio of atmospheric CO_2 while reducing CO_2 concentrations. This discrimination effect varies with photosynthetic pathway (C_3 versus C_4) and leaf environment (e.g., water stress). Respiration reverses this process, increasing CO_2 and decreasing the $^{13}C/^{12}C$ ratio of CO_2. A similar impact is produced by the burning of fossil fuels, which are ultimately formed from biomatter with a similar $^{13}C/^{12}C$ ratio. The $^{13}C/^{12}C$ ratio of CO_2 is not strongly influenced by net exchanges of CO_2 across the air-sea interface, but it is influenced by gross exchanges across the air-sea interface and with the land biosphere, which allow isotopic anomalies in the atmosphere to spread into the ocean and land biosphere. These types of isotopic exchanges, which swap atoms between reservoirs but entail no net CO_2 flux, are known as disequilibrium fluxes. Variations in $^{13}C/^{12}C$ ratio are typically reported in delta notation in permil, $\delta^{13}C = (r_{sample}/r_{standard} - 1) \times 1{,}000$, where r is the $^{13}C/^{12}C$ ratio and the standard is based on Pee Dee Belemnite carbonate.

Time-series measurements of $\delta^{13}C$ of atmospheric CO_2 began as a collaboration between Charles D. Keeling at Scripps and Wim Mook in Groningen in the late 1970s (78), and other groups in the 1980s and 1990s (39, 79, 80). Measurements from ice cores have allowed past variations in $\delta^{13}C$ to be reconstructed (17, 61). These measurements (**Figures 7** and **8**) show a rich spectrum of variability, including seasonal cycles, systematic gradients between the hemispheres, interannual variability associated with El Niño events, and a long-term downward trend, mirroring the rise in CO_2.

Figure 8 shows the main controls on the downward $\delta^{13}C$ trend. This trend is known as the ^{13}C-Suess effect, as it is driven by input of fossil-fuel CO_2 with slightly lower $^{13}C/^{12}C$ ratio, similar to the downward trend in $\Delta^{14}C$ from fossil-fuel burning. This trend is countered by the disequilibrium fluxes, which spread the ^{13}C-Suess effect into other reservoirs while reducing the Suess effect in the atmosphere by returning older carbon to the air. The downward trend is also countered by net uptake of CO_2 by land biota ($B - LU = 1.8$ Pg C/year; see **Table 1**), which thereby offsets the impact of fossil-fuel burning on both CO_2 amount and $\delta^{13}C$ of CO_2. The net uptake of anthropogenic CO_2 by the ocean has minimal impact on $\delta^{13}C$ of CO_2 (81).

An important early motivation for the $\delta^{13}C$ measurements was resolving the global land and ocean carbon sinks (82). The approach effectively solves for the land sink from the $\delta^{13}C$ trend, after correcting the trend for the fossil-fuel and disequilibrium flux contributions. The ocean sink is then resolved from the global balance (Equation 1). Sinks quantified by this approach are generally consistent with other methods (81, 83, 84); however, a significant complication involves

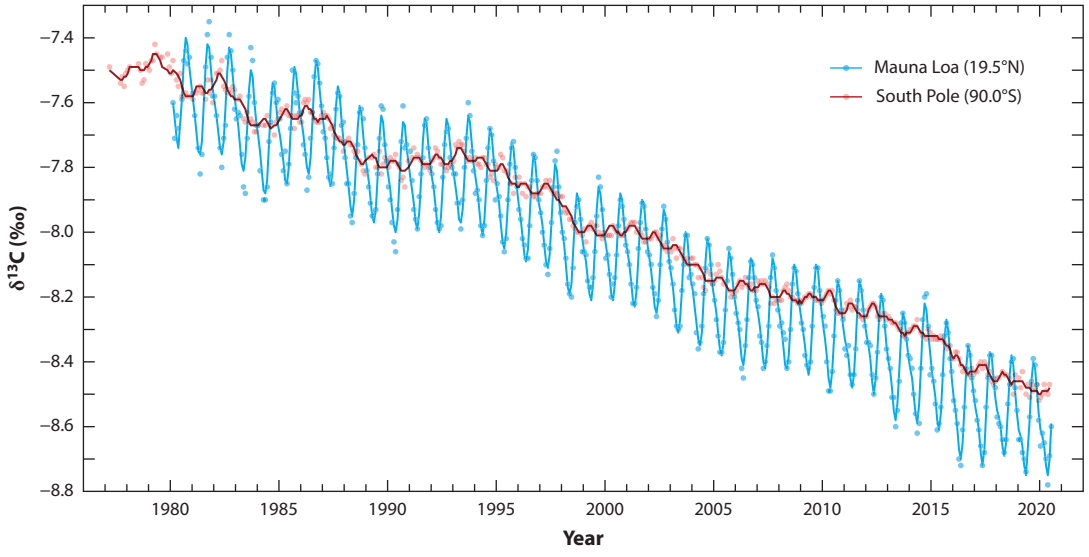

Figure 7

Monthly $\delta^{13}C$ of CO_2 as measured from flasks collected at Mauna Loa, Hawaii (19.5°N) and South Pole (90.0°S) observatories and analyzed by the Scripps CO_2 program.

uncertainty in the disequilibrium fluxes, which are sensitive to gross exchange rates as well as possible shifts in isotopic discrimination (74).

The approach can also be applied at smaller scales. For example, the interhemispheric $\delta^{13}C$ gradient, with lower $\delta^{13}C$ in the north mirroring the gradient in CO_2 (compare **Figures 1** and **7**),

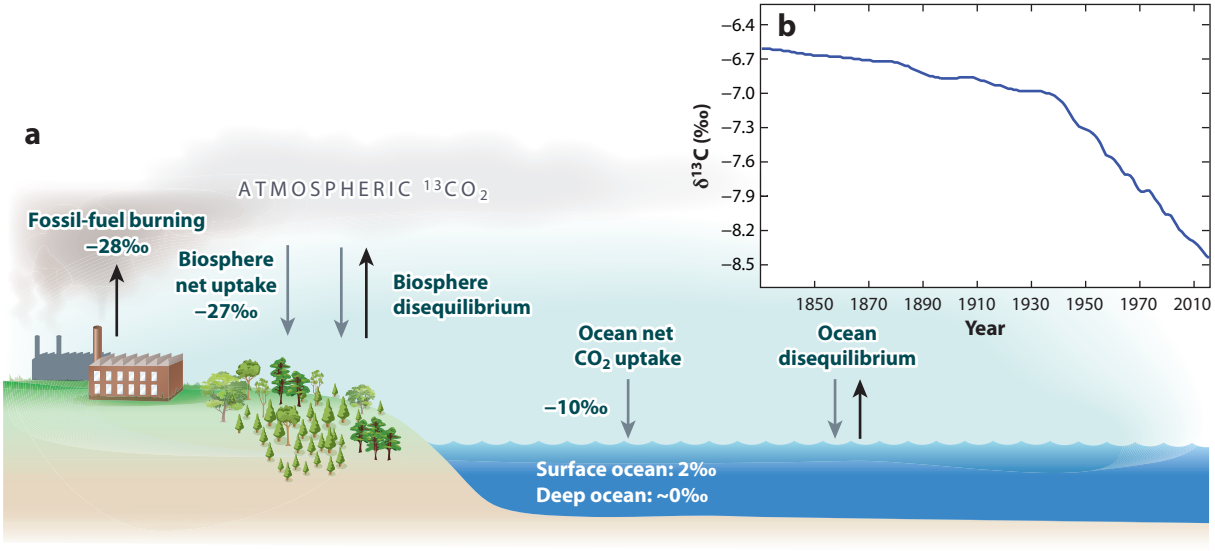

Figure 8

(*a*) Diagram of main controls on $\delta^{13}C$ of atmospheric CO_2 showing isotopic composition of net fluxes circa 1999 from Keeling et al. (74, table S5). (*b*) Global annual-mean $\delta^{13}C$, as presented in Graven et al. (12, 61).

has influences from fossil-fuel burning, oceanic exchanges, and biospheric exchanges and provides additional evidence in support of a northern land carbon sink (54).

On seasonal and interannual timescales, the variability of $\delta^{13}C$ of CO_2 is dominated by exchanges with land biota, producing tightly anticorrelated variations of $\delta^{13}C$ and CO_2. In the Northern Hemisphere, the combined seasonal cycles in $\delta^{13}C$ and CO_2 provide large-scale constraints on the isotopic discrimination of photosynthesis and their variations from year to year (78). The interannual variations in the downward $\delta^{13}C$ trend (**Figure 7**) have proved useful for confirming that land ecosystems are the dominant source of interannual variability in CO_2 (38, 39). Interannual variations in $\delta^{13}C$ are driven not only by interannual variations in net CO_2 flux but also by changes in $\delta^{13}C$ discrimination of land photosynthesis that covary with the driving processes, such as droughts. This covariation complicates the use of $\delta^{13}C$ data to resolve net land and ocean carbon fluxes on interannual timescales (85, 86).

Several recent studies have applied $\delta^{13}C$ data to resolve changes in photosynthetic discrimination rather than carbon sinks. For C_3 plants, discrimination is closely tied to intrinsic water-use efficiency (iWUE), a measure of photosynthetic carbon uptake per unit water loss. Keeling et al. (74) show that the long-term trend in $\delta^{13}C$ appears to require that discrimination has increased globally by 0.014 ± 0.007‰ per ppm CO_2, which is consistent with iWUE increasing roughly in proportion to atmospheric CO_2. Applications of atmospheric $\delta^{13}C$ data to resolve shifts in water-use efficiency have also been applied on smaller spatial scales (87, 88).

4. VARIATIONS IN ATMOSPHERIC O_2

The O_2 content of air is nearly constant at 21%, but varies measurably at the ppm level, providing information on carbon cycling and biogeochemistry. The main processes driving changes in O_2 are reactions involving production or destruction of organic carbon, such as photosynthesis, respiration, and fossil-fuel burning. These reactions produce O_2 while consuming CO_2, or vice versa, yielding opposing changes in O_2 and CO_2. The changes are much smaller in relative terms for O_2, due to its higher abundance in air (21% versus 0.04%). O_2 is not sensitive to the ocean carbonate chemistry reactions that buffer changes in atmospheric CO_2 nor to the disequilibrium fluxes that buffer changes in the isotopes of CO_2. Measurements of atmospheric O_2 can thus provide a distinct window on biogeochemical processes that is not available through measurements of CO_2 and its isotopes.

Changes in O_2 are typically reported as relative deviations in the O_2/N_2 ratio in per-meg units: $\delta(O_2/N_2) = (r_{sample}/r_{standard} - 1) \times 10^6$, where r is the O_2/N_2 ratio and the standard is archived natural air. Changes in $\delta(O_2/N_2)$ and CO_2 can be compared using a conversion factor of $1/0.2094 = 4.78$ per meg/ppm; i.e., converting 1 ppm of CO_2 into O_2 raises $\delta(O_2/N_2)$ by 4.78 per meg (0.2094 is the O_2 mole fraction of the standard).

Time-series measurements of changes in atmospheric O_2 began around 1990 and now include multiple international programs (13, 89, 90). **Figure 9** shows examples of time series from stations in the Northern and Southern Hemispheres. Major features include a decreasing trend, seasonal cycles with opposite phasing in the Northern and Southern Hemispheres (91, 92), and a north–south gradient with higher $\delta(O_2/N_2)$ on average in the south (92, 93).

The seasonal cycles in O_2/N_2 arise from exchanges of O_2 with terrestrial ecosystems and the oceans, which are largely in phase, releasing O_2 in summer and taking up O_2 in winter. The $\delta(O_2/N_2)$ cycles are larger than the cycles in CO_2 due to the larger oceanic component, especially in the Southern Hemisphere (89). Oceans release O_2 in spring and summer because O_2 is less soluble in warmer waters, marine phytoplankton produce more O_2 by photosynthesis, and vertical ocean mixing is more limited by warmer, more buoyant surface waters. These biological

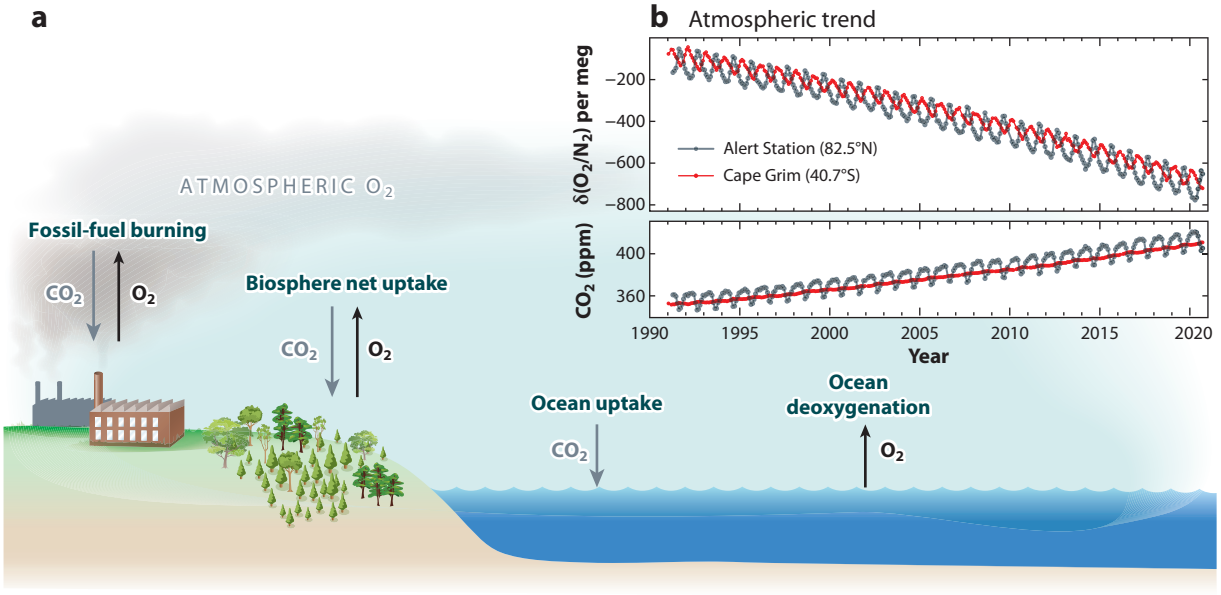

Figure 9

(*a*) Diagram of the coupled controls on atmospheric O_2 and CO_2. (*b*) Monthly $\delta(O_2/N_2)$ and CO_2 data in the Northern Hemisphere (Alert Station, 82.5°N) and Southern Hemisphere (Cape Grim, 40.7°S) from the Scripps O_2 program (**https://scrippso2.ucsd.edu/**).

and physical processes also drive changes in CO_2, but the resulting seasonal CO_2 exchanges are much smaller than those of O_2 because air-sea CO_2 exchange is slowed down by carbonate chemistry (94).

The global downward trend in $\delta(O_2/N_2)$ is driven by fossil-fuel burning, but it is counteracted by O_2 sources from the land and oceans:

$$M' \cdot d\delta(O_2/N_2)/dt = -\alpha_{FF} FF + \alpha_B (B - LU) + Z_{eff}, \qquad 2.$$

where FF, LU, and B are terms from the CO_2 budget in Pg C/year (Equation 1), α_B and α_{FF} are effective oxidative ratios (O_2:C) of the global net land sink and global fossil-fuel combustion, Z_{eff} is the effective ocean source of O_2, and M' is a unit conversion factor of 2.12/4.78 = 0.444 Pg (per meg)$^{-1}$. Equation 2 notably has no term corresponding to the ocean CO_2 sink nor any disequilibrium terms. The term Z_{eff} accounts for transient oceanic loss of O_2 driven by climate changes or anthropogenic nutrient inputs, which are tied to ocean deoxygenation (95). Z_{eff} also includes a small contribution from warming-induced loss of dissolved N_2.

A major application for $\delta(O_2/N_2)$ measurements is quantifying the global ocean carbon sink (O) and the net land sink ($B - LU$) by solving Equations 1 and 2 using estimates of the other quantities in these equations (13, 89). The oxidative ratio α_B is not measurable at global scales, but it must have a value near 1.1, similar to the ratio expected for major forms of biomatter (lignin, humins, etc.) (13). The oxidative ratio of fossil-fuel α_{FF} depends on fuel type (coal 1.17, petroleum 1.44, natural gas 1.95), recently averaging 1.38 globally (13). Z_{eff} is the smallest term in the budget, but it is not negligible. Z_{eff} has generally been estimated using a scaling relationship with ocean heat content (13). On timescales of a few years, the application of Equation 2 is complicated by uncertainties in the air-sea O_2 exchanges, but this complication is less serious on longer timescales (96). The uncertainties in the calculated decadal average land and ocean sinks are dominated by contributions from fossil-fuel burning and Z_{eff} (13). Using measurements of the $\delta(O_2/N_2)$ trend,

Ocean deoxygenation: ongoing loss of dissolved O_2 in the ocean interior related to climate change or other factors

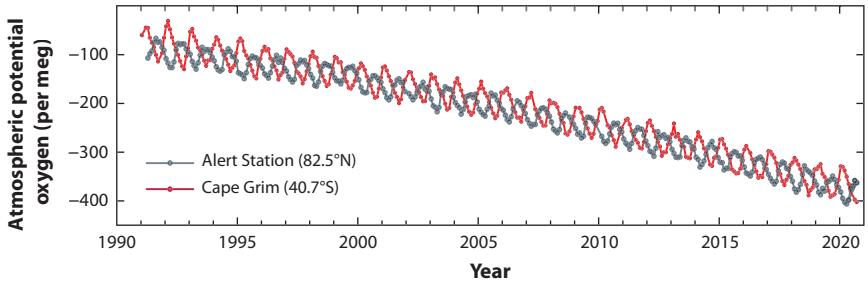

Figure 10

Monthly atmospheric potential oxygen (APO) data in the Northern Hemisphere (Alert Station, 82.5°N) and Southern Hemisphere (Cape Grim, 40.7°S) from the Scripps O_2 program.

Keeling & Manning (13) estimate an ocean sink of 1.9 ± 0.6 Pg C/year and net land sink ($B - LU$) of 1.2 ± 0.8 Pg C/year for the decade of the 1990s, in good agreement with independent estimates for this decade (10).

$\delta(O_2/N_2)$ measurements also provide unique signals of ocean biogeochemical processes. $\delta(O_2/N_2)$ and CO_2 data can be combined to compute atmospheric potential oxygen (APO), where APO = $\delta(O_2/N_2) + 1.1 \cdot 4.78\ CO_2$ (93). By design, APO removes the effect of exchanges with the land biosphere, which often dominate observed variability in O_2 and CO_2 but by virtue of the nearly fixed oxidative ratio of 1.1, produce compensating changes in $\delta(O_2/N_2)$ and CO_2. The APO concentration in air can be influenced by air-sea exchanges of CO_2, O_2, and N_2, as well as by O_2 and CO_2 exchanges caused by burning fossil fuels which have oxidative ratios higher than 1.1. The variations in APO can be corrected for the direct contributions of fossil-fuel burning, thus resolving residual changes driven by air-sea exchanges (93).

Figure 10 shows APO time series from flasks measured at Scripps from the Alert (82.5°N) and Cape Grim (40.7°S) stations. At both stations, seasonal cycles and a downward trend are visible. Because the seasonal air-sea exchanges of CO_2 and seasonal fossil-fuel contributions are small, the cycles of APO reflect the component of the O_2/N_2 cycle caused by air-sea exchanges. The global downward trend in APO results mainly from fossil-fuel combustion and long-term oceanic uptake of CO_2 and forms another basis for estimating the global ocean and land CO_2 sinks (13). The APO data also contain more subtle interannual signals tied mostly to changes in ventilation in various ocean basins, including the North Atlantic and Pacific (97), Equatorial Pacific (98, 99), and Southern Ocean (100).

APO measurements have helped to advance understanding of key carbon cycle processes, such as rates of ocean production and ventilation (89, 101, 102) and rates of air-sea gas exchange (91). They have also proved useful for testing of ocean biological models (93, 96, 103–106). APO measurements have also recently been applied to constrain long-term air-sea heat fluxes on hemispheric and global scales (107, 108), showing a resolvable signal of global ocean warming related to ocean deoxygenation (107).

Atmospheric potential oxygen (APO): the sum of O_2 and CO_2 concentrations, which is insensitive to land photosynthesis and respiration, thereby isolating oceanic processes

5. OXYGEN-18 IN CO_2 AND CARBONYL SULFIDE

We now turn to two tracers with geochemical similarities: the $^{18}O/^{16}O$ ratio of CO_2 and COS (carbonyl sulfide). The $^{18}O/^{16}O$ ratio measures the abundance of the $^{18}O^{12}C^{16}O$ isotopologue, in which one of the oxygen atoms is replaced with the rare isotope ^{18}O (comprising ~0.22% of oxygen atoms). COS is similar, with one oxygen atom instead replaced with sulfur. Changes in

$^{18}O/^{16}O$ are reported in delta notation, $\delta^{18}O$, similar to $^{13}C/^{12}C$, whereas COS is reported as mole fraction in parts-per-trillion.

The variability of $\delta^{18}O$ of CO_2 is controlled by exchanges with liquid water (109). CO_2 that is in contact with liquid water will tend to achieve both chemical and isotopic equilibrium with the water based on hydration reactions that exchange O atoms between H_2O and dissolved CO_2. The most important water reservoirs for CO_2 exchange are the oceans, soil water, and leaf water. Although the oceans are relatively homogeneous isotopically, the equilibrium fractionation depends on temperature (110). $\delta^{18}O$ in soil- and leaf-water reservoirs is highly variable due to fractionation of water isotopes during evaporation and precipitation (111, 112). These sources of variability are imparted onto variability in $\delta^{18}O$ of CO_2. Exchange of atmospheric CO_2 with leaf water occurs via CO_2 molecules that diffuse into leaves through stomata, equilibrate, and then diffuse back out again, escaping photosynthesis. Roughly two-thirds of the CO_2 molecules entering the stomata escape in this way (109). Exchange of CO_2 with soil water occurs either by diffusion of CO_2 into the soil and back out again or via a loop that involves CO_2 uptake by leaves, respiration below ground, and diffusion of CO_2 out of the soil (113, 114). In leaves and in some soils, the isotopic exchange is accelerated by the enzyme carbonic anhydrase, which catalyzes the hydration reaction (115, 116). The presence of carbonic anhydrase makes leaf water the most important reservoir for O-atom exchange. The lifetime of atmospheric oxygen atoms in CO_2 with respect to exchange with liquid water is estimated to be less than 1.9 years (117, 118).

The variability of COS is controlled by the balance of sources and sinks (14, 119). Major sources include the oceans, which release COS directly and indirectly (as a breakdown product of other sulfur gases), biomass burning, and anthropogenic emissions associated with synthetic fiber, aluminum, and coal industries. The primary sinks are uptake by terrestrial vegetation and soils where COS is hydrated and thereby destroyed (119, 120). The pathway for COS uptake in leaves is very similar to the pathway for $\delta^{18}O$, involving diffusion through stomata and hydration by carbonic anhydrase (121). Relatively minor contributions to the COS budget are made by emissions from volcanos, anoxic soils, wetlands, and removal by oxidation in the troposphere and stratosphere (122). COS has a relatively short lifetime of <2 years based mainly on the rapid hydration in leaves and soils (122). COS is climatically important as a source of stratospheric aerosol and as a greenhouse gas (123).

Time-series measurements began in the late 1970s for $\delta^{18}O$ (117) and in 2000 for COS (124). Variations in COS prior to 2000 have been recovered from air extracted from polar ice cores and firn, providing quasi-decadal resolution (122). Reconstruction of earlier changes in $\delta^{18}O$ has not been possible because ice cores do not preserve $\delta^{18}O$ of CO_2. **Figure 11** shows examples from time series from Barrow, Mauna Loa, and the South Pole.

Both tracers undergo seasonal cycles with larger cycles in the Northern Hemisphere. In the Southern Hemisphere, the oceans dominate the variability of COS, whereas the variability of $\delta^{18}O$ has both oceanic and terrestrial contributions. In the Northern Hemisphere, terrestrial exchanges dominate both signals (124, 125). In the summer, when vegetation is active, COS is removed and $\delta^{18}O$ of CO_2 is altered through exchanges with leaf and soil water. Particularly at high northern latitudes, leaf and soil water tends to be depleted in $\delta^{18}O$ leading to a summertime decrease in $\delta^{18}O$ of CO_2. This strong summertime exchange also leads to a gradient in annual-mean $\delta^{18}O$ of CO_2 within the Northern Hemisphere, with lower values in the north (109). The time series in **Figure 11** show little evidence for long-term trends in either $\delta^{18}O$ or COS, although $\delta^{18}O$ does vary interannually in association with El Niño events (117). The lack of a long-term trend in $\delta^{18}O$ is a reflection of the rapid turnover of O atoms with the water reservoirs overwhelming other influences such as emission of fossil-fuel CO_2, which is slightly depleted in $\delta^{18}O$ (109).

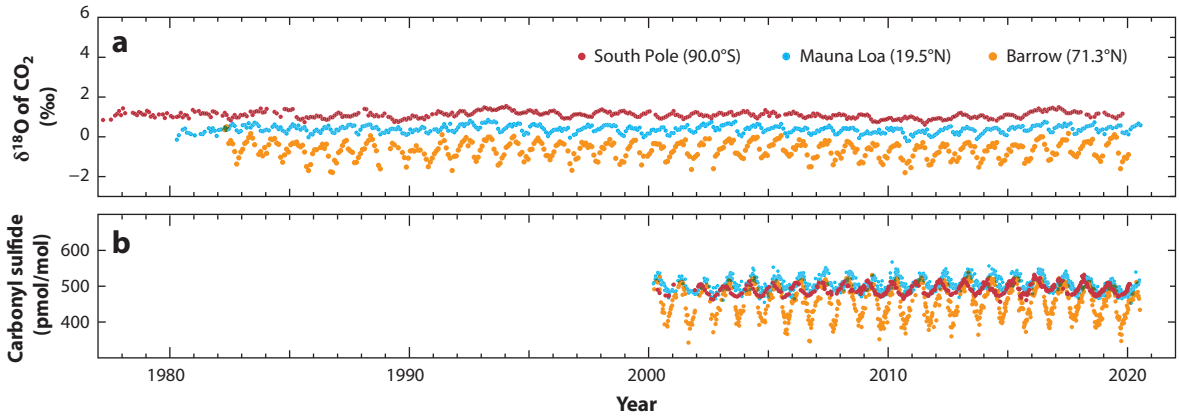

Figure 11

(*a*) $\delta^{18}O$ and (*b*) carbonyl sulfide (COS) data from Barrow (71.3°N), Mauna Loa, Hawaii (19.5°N), and the South Pole (90.0°S). Monthly $\delta^{18}O$ from the Scripps CO_2 program. COS measurements are averages of paired flask samples in parts-per-trillion (pmol mol^{-1}) collected every one to two weeks from National Oceanic and Atmospheric Administration Global Monitoring Laboratory (downloaded from **ftp://aftp.cmdl.noaa.gov/hats/carbonyl_sulfide**). These data extend the records published in Montzka et al. (124).

The Antarctic ice and firn records show COS rising from a preindustrial level of ~350 ppt to a maximum of ~550 ppt around 1990, and then roughly stabilizing over the next 10 years to current levels of 500 ppt. Greenland firn records show a similar pattern, but with an earlier peak circa 1975. These variations have been attributed to changing anthropogenic emissions of COS with the lifetime of COS remaining roughly constant (122).

Both tracers can potentially provide insights into leaf-level processes such as stomatal conductance and GPP of terrestrial vegetation. To date, global-scale applications have relied on particular signals that are interpretable despite the many potential complications (anthropogenic COS emissions, soil impacts, fractionation of water isotopes in the hydrological cycle). One such signal is the variability of $\delta^{18}O$ with El Niño events, which is driven by changes in tropical leaf- and soil-water $\delta^{18}O$ associated with variable tropical drought (117). There is a significant lag in the $\delta^{18}O$ response to El Niño that constrains the global turnover time of the O atom in CO_2, which is useful for constraining global GPP (117). GPP estimated using this approach is significantly higher than in previous studies (117). Another signal is the long-term trend in COS resolved from firn data, which appears to require a large increase in GPP since 1900 (126). The COS lifetime is proportional to CO_2/(GPP·LRU) where LRU (leaf relative uptake) is a measure of the relative uptake efficiency of COS versus CO_2 by vegetation (122). If LRU and the COS lifetime remained relatively constant over the twentieth century, then GPP must have increased roughly in proportion to atmospheric CO_2, corresponding to a 30% increase from 1900 to 2000 (126).

6. DISCUSSION AND OUTLOOK

We have reviewed results from long-term measurements of atmospheric CO_2 and related tracers in the atmosphere, which serve to document the rise in CO_2 and the exchanges of CO_2 with the land and oceans. The records have enabled a steady stream of scientific discoveries that were not anticipated at the time the measurements were initiated.

One of the most notable findings of these measurements is the surprisingly large changes in land ecosystems. The interhemispheric gradients in CO_2 and $\delta^{13}C$ indicate the presence of a

growing Northern Hemisphere land sink (53, 54), whereas the combined mass balance relationships for O_2 and CO_2 require a growing land sink at the global scale (127). The large changes in the seasonal cycle show that significant changes have occurred in net photosynthetic uptake of CO_2 in the summer (31) and in fall respiration (37). The carbon isotopic data help clarify that large-scale changes in water-use efficiency have accompanied the rise in CO_2 (74) and the COS data support a large increase in GPP (126). These large changes, which were partly unanticipated by ecologists (e.g., 128), have played a major role in motivating research into the terrestrial carbon cycle in recent years.

In contrast, long-term atmospheric measurements have led to fewer surprises regarding the behavior of the oceans. The data strongly support theories already advanced in the 1950s that the ocean sink would be dominated by physical dissolution of CO_2 in the ocean and physical transport into the interior (129). Marine organisms are now under the triple threat of ocean warming, acidification, and deoxygenation (130). But other than the signal of ocean warming and deoxygenation that has emerged from the APO trend (95, 107), and the ocean acidification implied by the CO_2 uptake, no other major indicators of marine ecological changes are evident in the atmospheric records. The seasonal cycles in APO, for example, show no clear evidence of hemispheric-scale trends from 1990 to present, and thus no major changes in marine productivity or seasonal ventilation over this period. We know from long-term observations of CO_2 in the surface ocean that significant variability in oceanic CO_2 uptake occurs at the scale of individual basins over a range of timescales, and this variability must contribute to global variability in CO_2 (131, 132). But a signal of these processes has not yet been clearly resolved in the global trends of CO_2 or its isotopes.

An important result is the finding that the sinks for CO_2 have been growing roughly in proportion to emissions over the past sixty years. In simple models, a relatively constant airborne fraction is expected from the quasi-exponential growth of emissions, which leads to relatively constant partitioning of the excess CO_2 across land, ocean, and atmospheric reservoirs (15, 129). Assuming emissions eventually plateau, a decreasing airborne fraction is expected, as the sinks depend on the full emissions history rather than current emissions (133). For example, a rapid drop in emissions does not imply an equally rapid drop in the sinks. The long-term sink behavior will depend strongly on the future emissions pathway, eventually weakening or possibly reversing if CO_2 drops sufficiently (134).

The discovery of new phenomena through these datasets will almost certainly continue. As the records grow in length, new signals have emerged. Just within the past decade, a possible signal of secular changes in the El Niño impacts on CO_2 has emerged (135), as have El Niño signals in ^{18}O of CO_2 (117) and signals of long-term increasing water-use efficiency of land ecosystems from $\delta^{13}C$ (74). In time, we may discover clear signals in changing ocean biogeochemistry through APO, feedbacks between climate change and carbon fluxes with the oceans or permafrost through $\Delta^{14}C$ (12), or better constraints on trends in gross or net primary production of land ecosystems through COS and $\delta^{18}O$. We still await positive detection of a change in the airborne fraction.

In this review, we have not attempted to describe phenomena on small space- or timescales. In this context, an important direction of ongoing research is the creation of denser sampling networks, taking advantage of new technologies for in situ, satellite, and column-measurement approaches (136–138). At present, our knowledge of long-term trends in CO_2 and related species is mostly based on air samples that were collected weekly or monthly in flasks and shipped to a central laboratory for analysis. A massive improvement in temporal resolution is now possible by deploying in situ analyzers that employ laser-based and other novel measurement technologies to measure every second or minute. Data assimilation systems using inverse modeling to derive surface fluxes or constrain the controlling processes on land or in the ocean are becoming

more advanced (139, 140). Nevertheless, the development of assimilation systems that fully utilize the multi-tracer constraints is still in the early stages (75, 141), as are the observations of changes in rarer CO_2 isotopologues, such as $^{13}C^{18}O^{16}O$ or $^{12}C^{17}O^{16}O$, which may provide further constraints on carbon cycling (142).

Sustained measurements of atmospheric CO_2 and related tracers provide the foundation of carbon cycle research, and they are as important now as ever. Many processes in the carbon cycle are still not well understood, such as the land CO_2 sink, which means that future projections of atmospheric CO_2 and climate change span large potential ranges. Continuing these observations and using them in innovative new studies will be fundamental to advancing the state of the science. CO_2 and related tracer measurements are also critical for the detection of feedbacks of climate changes on carbon sinks, which may significantly modify the climate response to fossil-fuel emissions (143). As the world takes steps to mitigate climate change, a sustained slowing in the CO_2 growth rate observed at Mauna Loa will be necessary to show that mitigation measures are effective.

SUMMARY POINTS

1. The buildup of atmospheric CO_2 from fossil-fuel burning and land use has been offset by approximately 50% by land and ocean sinks, which have grown roughly proportionally with emissions over the past 60 years.
2. A large increase in the amplitude in the CO_2 seasonal cycle has been detected since the 1960s in high northern latitudes, which indicates widespread changes have occurred in boreal and temperate terrestrial ecosystems.
3. The growth rate of CO_2 has fluctuated on interannual timescales, mainly as a result of variations in the growth and decay of tropical biomass tied to moisture and temperature variations.
4. The Northern Hemisphere contains an annual excess of several ppm CO_2 compared to the Southern Hemisphere. The excess is driven by fossil-fuel burning, which is concentrated in the North, but it is partly counteracted by a northern land sink for CO_2 which has grown roughly in proportion to fossil-fuel emissions.
5. The radiocarbon content of CO_2 ($^{14}C/C$) increased following the atmospheric atom-bomb tests of the 1950s and 1960s, but has decreased since then, as the bomb excess ^{14}C has spread into the oceans and land reservoirs, and as fossil-fuel emissions have injected ^{14}C-free CO_2 into the atmosphere. Measurements of radiocarbon have proved critical for quantifying CO_2 exchange rates between reservoirs and quantifying fossil-fuel emissions.
6. The $^{13}C/^{12}C$ ratio of CO_2 has decreased over the past century due to the burning of fossil fuels with low $^{13}C/^{12}C$ ratios. $^{13}C/^{12}C$ measurements are useful for quantifying land carbon sinks and resolving changes in the water-use efficiency of land photosynthesis.
7. The atmospheric O_2/N_2 ratio has decreased in concert with the rise in CO_2 because O_2 is consumed by fossil-fuel burning. Measurements of O_2/N_2 provide unique insights into land and ocean carbon sinks and changing ocean biogeochemistry.
8. Measurements of carbonyl sulfide and the $^{18}O/^{16}O$ ratio of CO_2 provide insights on the global rate of photosynthesis by land plants and its change over time.

FUTURE ISSUES

1. Continued measurements of CO_2 and related tracers are vital for assessing progress toward climate mitigation and detection of climate feedbacks impacting CO_2 buildup.
2. Time-series measurements of O_2 are poised to provide novel insights changing ocean biogeochemistry, similar to the role played by CO_2 and its isotopes in the detection of changing land biogeochemistry.
3. An important goal is the monitoring of trends in the airborne fraction. As fossil-fuel emissions eventually plateau and decrease, the airborne fraction is expected to decrease.
4. Opportunities for vast improvements in measurement quality and data density for CO_2 and related tracers are possible by employment of novel measurement techniques based on lasers and other technologies.
5. Major insights into the carbon cycle may be achieved through the development of models that assimilate not just CO_2 data, but also data for carbon isotopes, O_2, and COS.

DISCLOSURE STATEMENT

The authors are not aware of any affiliations, memberships, funding, or financial holdings that might be perceived as affecting the objectivity of this review.

ACKNOWLEDGMENTS

We thank Wouter Peters, Britton Stephens, and John Miller for significant help in reviewing the article. The Scripps O_2 and CO_2 programs have been supported by a series of grants from the National Science Foundation, Department of Energy, National Oceanic and Atmospheric Administration, and National Aeronautics and Space Administration, most recently by NA20OAR4320278, OPP-1922922, and NNX17AE74G. H.D.G. acknowledges support from the Leverhulme Trust.

LITERATURE CITED

1. Revelle R, Broecker W, Craig H, Keeling CD, Smagorinsky J. 1965. Atmospheric carbon dioxide. In *Report of the Environmental Pollution Panel President's Advisory Committee, November 1965*, pp. 111–33. Washington, DC: The White House
2. Keeling CD, Adams JA Jr., Ekdahl CA Jr., Guenther PR. 1976. Atmospheric carbon dioxide variations at the South Pole. *Tellus* 28:552–64
3. Bacastow RB. 1976. Modulation of atmospheric carbon dioxide by the Southern Oscillation. *Nature* 261:116–18
4. Pearman GI, Hyson P. 1980. Activities of the global biosphere as reflected in atmospheric CO_2 records. *J. Geophys. Res. Oceans* 85:4457–67
5. Keeling RF, Piper SC, Heimann M. 1996. Global and hemispheric CO_2 sinks deduced from changes in atmospheric O_2 concentration. *Nature* 381:218–21
6. Tans PP, Conway TJ, Nakazawa T. 1989. Latitudinal distribution of the source and sinks of atmospheric carbon dioxide derived from surface observations and an atmospheric transport model. *J. Geophys. Res. Atmos.* 94:5151–73
7. Tans PP, Fung IY, Takahashi T. 1990. Observational constraints on the global atmospheric CO_2 budget. *Science* 247:1431–38

8. Ciais P, Tans PP, Trolier M, White JWC, Francey RJ. 1995. A large northern-hemisphere terrestrial CO_2 sink indicated by the $^{13}C/^{12}C$ ratio of atmospheric CO_2. *Science* 269:1098–102
9. Ballantyne AP, Alden CB, Miller JB, Tans PP, White JWC. 2012. Increase in observed net carbon dioxide uptake by land and oceans during the past 50 years. *Nature* 488:70–73
10. Friedlingstein P, O'Sullivan M, Jones MW, Andrew RM, Hauck J, et al. 2020. Global carbon budget 2020. *Earth Syst. Sci. Data* 12:3269–340
11. Graven HD. 2016. The carbon cycle in a changing climate. *Phys. Today* 69:48–54
12. Graven H, Keeling RF, Rogelj J. 2020. Changes to carbon isotopes in atmospheric CO_2 over the Industrial Era and into the future. *Glob. Biogeochem. Cycle* 34:e2019GB006170
13. Keeling RF, Manning AC. 2014. Studies of recent changes in atmospheric O_2 content. In *Treatise on Geochemistry*, Vol. 5: *The Atmosphere*, ed. RF Keeling, L Russell, pp. 385–404. Amsterdam: Elsevier. 2nd ed.
14. Whelan M, Lennartz S, Gimeno T, Wehr R, Wohlfahrt G, et al. 2018. Reviews and syntheses: carbonyl sulfide as a multi-scale tracer for carbon and water cycles. *Biogeosciences* 15:3625–57
15. Keeling CD, Whorf TP, Wahlen M, van der Plichtt J. 1995. Interannual extremes in the rate of rise of atmospheric carbon dioxide since 1980. *Nature* 375:666–70
16. WMO (World Meteorol. Organ.). 2018. *The state of greenhouse gases in the atmosphere based on global observations through 2017*. WMO Greenh. Gas Bull. 14, WMO, Geneva
17. Rubino M, Etheridge DM, Thornton DP, Howden R, Allison CE, et al. 2019. Revised records of atmospheric trace gases CO_2, CH_4, N_2O, and $\delta^{13}C$-CO_2 over the last 2000 years from Law Dome, Antarctica. *Earth Syst. Sci. Data* 11:473–92
18. Luthi D, Le Floch M, Bereiter B, Blunier T, Barnola JM, et al. 2008. High-resolution carbon dioxide concentration record 650,000–800,000 years before present. *Nature* 453:379–82
19. Patra P, Takigawa M, Dutton G, Uhse K, Ishijima K, et al. 2009. Transport mechanisms for synoptic, seasonal and interannual SF_6 variations and "age" of air in troposphere. *Atmos. Chem. Phys.* 9:1209–15
20. Rafelski LE, Piper SC, Keeling RF. 2009. Climate effects on atmospheric carbon dioxide over the last century. *Tellus B.* 61:718–31
21. Knorr W. 2009. Is the airborne fraction of anthropogenic CO_2 emissions increasing? *Geophys. Res. Lett.* 36:L21710
22. Walker AP, De Kauwe MG, Bastos A, Belmecheri S, Georgiou K, et al. 2021. Integrating the evidence for a terrestrial carbon sink caused by increasing atmospheric CO_2. *New Phytol.* 229:2413–45
23. Huntzinger D, Michalak A, Schwalm C, Ciais P, King AW, et al. 2017. Uncertainty in the response of terrestrial carbon sink to environmental drivers undermines carbon-climate feedback predictions. *Sci. Rep.* 7:4765
24. Fu Z, Dong J, Zhou Y, Stoy PC, Niu S. 2017. Long term trend and interannual variability of land carbon uptake—the attribution and processes. *Environ. Res. Lett.* 12:014018
25. Keeling CD. 1960. The concentration and isotopic abundances of carbon dioxide in the atmosphere. *Tellus* 12:200–3
26. Heimann M, Keeling CD, Tucker CJ. 1989. A three-dimensional model of atmospheric CO_2 transport based on observed winds: 3. Seasonal cycle and synoptic time scale variations. In *Aspects of Climate Variability in the Pacific and the Western Americas*, Vol. 55, ed. DH Peterson, pp. 277–303. Washington, DC: Am. Geophys. Union
27. Pearman GI, Hyson P. 1981. The annual variation of atmospheric CO_2 concentration observed in the northern hemisphere. *J. Geophys. Res. Oceans* 86:9839–43
28. Bacastow RB, Keeling CD, Whorf TP. 1985. Seasonal amplitude increase in atmospheric CO_2 concentration at Mauna Loa, Hawaii, 1959–1982. *J. Geophys. Res. Atmos.* 90:10529–40
29. Keeling CD, Chin JFS, Whorf TP. 1996. Increased activity of northern vegetation inferred from atmospheric CO_2 measurements. *Nature* 382:146–49
30. Randerson JT, Thompson MV, Conway TJ, Fung IY, Field CB. 1997. The contribution of terrestrial sources and sinks to trends in the seasonal cycle of atmospheric carbon dioxide. *Glob. Biogeochem. Cycle* 11:535–60

31. Graven HD, Keeling RF, Piper SC, Patra PK, Stephens BB, et al. 2013. Enhanced seasonal exchange of CO_2 by northern ecosystems since 1960. *Science* 341:1085–89
32. Forkel M, Carvalhais N, Rödenbeck C, Keeling R, Heimann M, et al. 2016. Enhanced seasonal CO_2 exchange caused by amplified plant productivity in northern ecosystems. *Science* 351:696–99
33. Lin X, Rogers BM, Sweeney C, Chevallier F, Arshinov M, et al. 2020. Siberian and temperate ecosystems shape Northern Hemisphere atmospheric CO_2 seasonal amplification. *PNAS* 117:21079–87
34. Thomas RT, Prentice LC, Graven H, Ciais P, Fisher JB, et al. 2016. Increased light-use efficiency in northern terrestrial ecosystems indicated by CO_2 and greening observations. *Geophys. Res. Lett.* 43:11339–49
35. Haverd V, Smith B, Canadell JG, Cuntz M, Mikaloff Fletcher SE, et al. 2020. Higher than expected CO_2 fertilization inferred from leaf to global observations. *Glob. Change Biol.* 26:2390–402
36. Randerson JT, Field CB, Fung IY, Tans PP. 1999. Increases in early season ecosystem uptake explain recent changes in the seasonal cycle of atmospheric CO_2 at high northern latitudes. *Geophys. Res. Lett.* 26:2765–68
37. Piao SL, Ciais P, Friedlingstein P, Peylin P, Reichstein M, et al. 2008. Net carbon dioxide losses of northern ecosystems in response to autumn warming. *Nature* 451:49–52
38. Keeling CD, Revelle R. 1985. Effects of El Nino/Southern Oscillation on the atmospheric content of carbon dioxide. *Meteoritics* 20:437–50
39. Nakazawa T, Morimoto S, Aoki S, Tanaka M. 1993. Time and space variations of the carbon isotopic ratio of tropospheric carbon dioxide over Japan. *Tellus B*. 45:258–74
40. Bousquet P, Peylin P, Ciais P, Le Quéré C, Friedlingstein P, Tans PP. 2000. Regional changes in carbon dioxide fluxes of land and oceans since 1980. *Science* 290:1342–46
41. Jones CD, Collins M, Cox PM, Spall SA. 2001. The carbon cycle response to ENSO: a coupled climate-carbon cycle model study. *J. Climate* 14:4113–29
42. Feely RA, Wanninkhof R, Takahashi T, Tans P. 1999. Influence of El Niño on the equatorial Pacific contribution to atmospheric CO_2 accumulation. *Nature* 398:597–601
43. Ahlström A, Raupach MR, Schurgers G, Smith B, Arneth A, et al. 2015. The dominant role of semi-arid ecosystems in the trend and variability of the land CO_2 sink. *Science* 348:895–99
44. Poulter B, Frank D, Ciais P, Myneni RB, Andela N, et al. 2014. Contribution of semi-arid ecosystems to interannual variability of the global carbon cycle. *Nature* 509:600–3
45. Cox PM, Pearson D, Booth BB, Friedlingstein P, Huntingford C, et al. 2013. Sensitivity of tropical carbon to climate change constrained by carbon dioxide variability. *Nature* 494:341–44
46. Jung M, Reichstein M, Schwalm CR, Huntingford C, Sitch S, et al. 2017. Compensatory water effects link yearly global land CO_2 sink changes to temperature. *Nature* 541:516–20
47. Humphrey V, Zscheischler J, Ciais P, Gudmundsson L, Sitch S, Seneviratne SI. 2018. Sensitivity of atmospheric CO_2 growth rate to observed changes in terrestrial water storage. *Nature* 560:628–31
48. Brovkin V, Loren S, Jungclaus J, Raddatz T, Timmreck C, et al. 2010. Sensitivity of a coupled climate-carbon cycle model to large volcanic eruptions during the last millennium. *Tellus B*. 62:674–81
49. Angert A, Biraud S, Bonfils C, Buermann W, Fung I. 2004. CO_2 seasonality indicates origins of post-Pinatubo sink. *Geophys. Res. Lett.* 31:L11103
50. Bastos A, Ciais P, Barichivich J, Bopp L, Brovkin V, et al. 2016. Re-evaluating the 1940s CO_2 plateau. *Biogeosciences* 13:4877–97
51. Ballantyne A, Smith W, Anderegg W, Kauppi P, Sarmiento J, et al. 2017. Accelerating net terrestrial carbon uptake during the warming hiatus due to reduced respiration. *Nat. Climate Change* 7:148–52
52. Fan S-M, Blaine TL, Sarmiento JL. 1999. Terrestrial carbon sink in the Northern Hemisphere estimated from the atmospheric CO_2 difference between Mauna Loa and the South Pole since 1959. *Tellus B*. 51:863–70
53. Ciais P, Tan J, Wang X, Roedenbeck C, Chevallier F, et al. 2019. Five decades of northern land carbon uptake revealed by the interhemispheric CO_2 gradient. *Nature* 568:221–25
54. Keeling CD, Piper SC, Whorf TP, Keeling RF. 2011. Evolution of natural and anthropogenic fluxes of atmospheric CO_2 from 1957 to 2003. *Tellus B*. 63:1–22

55. Resplandy L, Keeling RF, Roedenbeck C, Stephens BB, Khatiwala S, et al. 2018. Revision of global carbon fluxes based on a reassessment of oceanic and riverine carbon transport. *Nat. Geosci.* 11:504–8
56. Keeling CD, Piper SC, Heimann M. 1989. A three-dimensional model of atmospheric CO_2 transport based on observed winds: 4. Mean annual gradients and interannual variations. In *Aspects of Climate Variability in the Pacific and the Western Americas*, Vol. 55, ed. DH Peterson, pp. 305–63. Washington, DC: Am. Geophys. Union
57. Stuiver M, Pollach HA. 1977. Discussion: Reporting of ^{14}C data. *Radiocarbon* 19:355–63
58. Rafter T, Fergusson G. 1957. "Atom bomb effect"—recent increase of carbon-14 content of the atmosphere and biosphere. *Science* 126:557–58
59. Nydal R, Lövseth K. 1983. Tracing bomb ^{14}C in the atmosphere 1962–1980. *J. Geophys. Res. Oceans* 88:3621–42
60. Levin I, Naegler T, Kromer B, Diehl M, Francey RJ, et al. 2010. Observations and modelling of the global distribution and long-term trend of atmospheric $^{14}CO_2$. *Tellus B.* 62:26–46
61. Graven H, Allison CE, Etheridge DM, Hammer S, Keeling RF, et al. 2017. Compiled records of carbon isotopes in atmospheric CO_2 for historical simulations in CMIP6. *Geosci. Model Dev.* 10:4405–17
62. Turnbull JC, Mikaloff Fletcher SE, Brailsford GW, Moss RC, Norris MW, Steinkamp K. 2017. Sixty years of radiocarbon dioxide measurements at Wellington, New Zealand: 1954–2014. *Atmos. Chem. Phys.* 17:14771–84
63. Van de Wal R, Meijer H, De Rooij M, Van der Veen C. 2007. Radiocarbon analyses along the EDML ice core in Antarctica. *Tellus B.* 59:157–65
64. Reimer PJ, Bard E, Bayliss A, Beck JW, Blackwell PG, et al. 2013. IntCal13 and Marine13 radiocarbon age calibration curves 0–50,000 years cal BP. *Radiocarbon* 55:1869–87
65. Suess HE. 1955. Radiocarbon concentration in modern wood. *Science* 122:415–17
66. Graven HD, Guilderson TP, Keeling RF. 2012. Observations of radiocarbon in CO_2 at La Jolla, California, USA 1992–2007: analysis of the long-term trend. *J. Geophys. Res. Atmos.* 117:D02302
67. Graven HD, Guilderson TP, Keeling RF. 2012. Observations of radiocarbon in CO_2 at seven global sampling sites in the Scripps flask network: analysis of spatial gradients and seasonal cycles. *J. Geophys. Res. Atmos.* 117:D02303
68. Hesshaimer V, Heimann M, Levin I. 1994. Radiocarbon evidence for a smaller oceanic carbon dioxide sink than previously believed. *Nature* 370:201–3
69. Sweeney C, Gloor E, Jacobson AR, Key RM, McKinley G, et al. 2007. Constraining global air-sea gas exchange for CO_2 with recent bomb ^{14}C measurements. *Glob. Biogeochem. Cycle* 21:GB2015
70. Wanninkhof R. 2014. Relationship between wind speed and gas exchange over the ocean revisited. *Limnol. Oceanogr. Methods* 12:351–62
71. Naegler T. 2009. Reconciliation of excess ^{14}C-constrained global CO_2 piston velocity estimates. *Tellus B.* 61:372–84
72. Naegler T, Levin I. 2006. Closing the global radiocarbon budget 1945–2005. *J. Geophys. Res. Atmos.* 111:D12311
73. Naegler T, Levin I. 2009. Biosphere-atmosphere gross carbon exchange flux and the $\delta^{13}CO_2$ and $\Delta^{14}CO_2$ disequilibria constrained by the biospheric excess radiocarbon inventory. *J. Geophys. Res. Atmos.* 114:D17303
74. Keeling RF, Graven HD, Welp LR, Resplandy L, Bi J, et al. 2017. Atmospheric evidence for a global secular increase in carbon isotopic discrimination of land photosynthesis. *PNAS* 114:10361–66
75. Basu S, Lehman SJ, Miller JB, Andrews AE, Sweeney C, et al. 2020. Estimating US fossil fuel CO_2 emissions from measurements of ^{14}C in atmospheric CO_2. *PNAS* 117:13300–7
76. Graven H, Fischer ML, Lueker T, Jeong S, Guilderson TP, et al. 2018. Assessing fossil fuel CO_2 emissions in California using atmospheric observations and models. *Environ. Res. Lett.* 13:065007
77. Miller JB, Lehman SJ, Verhulst KR, Miller CE, Duren RM, et al. 2020. Large and seasonally varying biospheric CO_2 fluxes in the Los Angeles megacity revealed by atmospheric radiocarbon. *PNAS* 117:26681–87
78. Keeling CD, Piper SC, Bacastow RB, Wahlen M, Whorf TP, et al. 2005. Atmospheric CO_2 and $^{13}CO_2$ exchange with the terrestrial biosphere and oceans from 1978 to 2000: observations and carbon cycle

implications. In *A History of Atmospheric CO_2 and Its Effects on Plants, Animals, and Ecosystems*, ed. JR Ehleringer, TE Cerling, MD Dearing, pp. 83–113. New York: Springer
79. Vaughn BH, Evans CU, White JW, Still CJ, Masarie KA, Turnbull J. 2010. Global network measurements of atmospheric trace gas isotopes. In *Isoscapes*, ed. JB West, GJ Bowen, TE Dawson, KP Tu, pp. 3–31. New York: Springer
80. Allison CE, Francey RJ. 2007. Verifying Southern Hemisphere trends in atmospheric carbon dioxide stable isotopes. *J. Geophys. Res. Atmos.* 112:D21304
81. Tans PP, Berry JA, Keeling RF. 1993. Oceanic $^{13}C/^{12}C$ observations: a new window on ocean CO_2 uptake. *Glob. Biogeochem. Cycle* 7:353–68
82. Keeling CD. 1979. The Suess effect: ^{13}carbon-^{14}carbon interrelations. *Environ. Int.* 2:229–300
83. Quay PD, Tilbrook B, Wong CS. 1992. Oceanic uptake of fossil fuel CO_2: carbon-13 evidence. *Science* 256:74–79
84. Trudinger C, Enting I, Etheridge D, Francey R, Rayner P. 2005. The carbon cycle over the past 1000 years inferred from the inversion of ice core data. In *A History of Atmospheric CO_2 and Its Effects on Plants, Animals, and Ecosystems*, ed. JR Ehleringer, TE Cerling, MD Dearing, pp. 329–49. New York: Springer
85. Randerson JT, Collatz GJ, Fessenden JE, Munoz AD, Still CJ, et al. 2002. A possible global covariance between terrestrial gross primary production and ^{13}C discrimination: consequences for the atmospheric ^{13}C budget and its response to ENSO. *Glob. Biogeochem. Cycle* 16:1136
86. Scholze M, Ciais P, Heimann M. 2008. Modeling terrestrial ^{13}C cycling: climate, land use and fire. *Glob. Biogeochem. Cycle* 22:GB1009
87. Ballantyne AP, Miller JB, Tans PP. 2010. Apparent seasonal cycle in isotopic discrimination of carbon in the atmosphere and biosphere due to vapor pressure deficit. *Glob. Biogeochem. Cycle* 24:GB3018
88. Peters W, van der Velde IR, Van Schaik E, Miller JB, Ciais P, et al. 2018. Increased water-use efficiency and reduced CO_2 uptake by plants during droughts at a continental scale. *Nat. Geosci.* 11:744–48
89. Keeling RF, Shertz SR. 1992. Seasonal and interannual variations in atmospheric oxygen and implications for the global carbon cycle. *Nature* 358:723–27
90. Tohjima Y, Mukai H, Machida T, Hoshina Y, Nakaoka S-I. 2019. Global carbon budgets estimated from atmospheric O_2/N_2 and CO_2 observations in the western Pacific region over a 15-year period. *Atmos. Chem. Phys.* 19:9269–85
91. Keeling RF, Stephens BB, Najjar RG, Doney SC, Archer D, Heimann M. 1998. Seasonal variations in the atmospheric O_2/N_2 ratio in relation to the kinetics of air-sea gas exchange. *Glob. Biogeochem. Cycle* 12:141–63
92. Tohjima Y, Mukai H, Machida T, Nojiri Y, Gloor M. 2005. First measurements of the latitudinal atmospheric O_2 and CO_2 distributions across the western Pacific. *Geophys. Res. Lett.* 32:L17805
93. Stephens BB, Keeling RF, Heimann M, Six KD, Murnane R, Caldeira K. 1998. Testing global ocean carbon cycle models using measurements of atmospheric O_2 and CO_2 concentration. *Glob. Biogeochem. Cycle* 12:213–30
94. Keeling RF, Najjar RP, Bender ML, Tans PP. 1993. What atmospheric oxygen measurements can tell us about the global carbon cycle. *Glob. Biogeochem. Cycle* 7:37–67
95. Keeling RF, Kortzinger A, Gruber N. 2010. Ocean deoxygenation in a warming world. *Annu. Rev. Mar. Sci.* 2:199–229
96. Nevison CD, Mahowald NM, Doney SC, Lima ID, Cassar N. 2008. Impact of variable air-sea O_2 and CO_2 fluxes on atmospheric potential oxygen (APO) and land-ocean carbon sink partitioning. *Biogeosciences* 5:875–89
97. Hamme RC, Keeling RF. 2008. Ocean ventilation as a driver of interannual variability in atmospheric potential oxygen. *Tellus B.* 60:706–17
98. Rődenbeck C, Le Quéré C, Heimann M, Keeling RF. 2008. Interannual variability in oceanic biogeochemical processes inferred by inversion of atmospheric O_2/N_2 and CO_2 data. *Tellus B.* 60:685–705
99. Eddebbar YA, Long MC, Resplandy L, Rodenbeck C, Rodgers KB, et al. 2017. Impacts of ENSO on air-sea oxygen exchange: observations and mechanisms. *Glob. Biogeochem. Cycle* 31:901–21
100. Nevison CD, Munro DR, Lovenduski NS, Keeling RF, Manizza M, et al. 2020. Southern Annular Mode influence on wintertime ventilation of the Southern Ocean detected in atmospheric O_2 and CO_2 measurements. *Geophys. Res. Lett.* 47:e2019GL085667

101. Jin X, Najjar RG, Louanchi F, Doney SC. 2007. A modeling study of the seasonal oxygen budget of the global ocean. *J. Geophys. Res. Oceans* 112:C05017
102. Nevison CD, Keeling RF, Kahru M, Manizza M, Mitchell BG, Cassar N. 2012. Estimating net community production in the Southern Ocean based on atmospheric potential oxygen and satellite ocean color data. *Glob. Biogeochem. Cycle* 26:GB1020
103. Gruber N, Gloor M, Fan SM, Sarmiento JL. 2001. Air-sea flux of oxygen estimated from bulk data: implications for the marine and atmospheric oxygen cycles. *Glob. Biogeochem. Cycle* 15:783–803
104. McKinley GA, Follows M, Marshal J. 2003. Interannual variability of air-sea O_2 fluxes and the determination of CO_2 sinks using atmospheric O_2/N_2. *Geophys. Res. Lett.* 30:1101
105. Naegler T, Ciais P, Orr JC, Aumont O, Rodenbeck C. 2007. On evaluating ocean models with atmospheric potential oxygen. *Tellus B*. 59:138–56
106. Battle M, Mikaloff Fletcher SE, Bender ML, Keeling RF, Manning AC, et al. 2006. Atmospheric potential oxygen: new observations and their implications for some atmospheric and oceanic models. *Glob. Biogeochem. Cycle* 20:GB1010
107. Resplandy L, Keeling RF, Eddebbar Y, Brooks M, Wang R, et al. 2019. Quantification of ocean heat uptake from changes in atmospheric O_2 and CO_2 composition. *Sci. Rep.* 9:20244
108. Resplandy L, Keeling RF, Stephens BB, Bent JD, Jacobson A, et al. 2016. Constraints on oceanic meridional heat transport from combined measurements of oxygen and carbon. *Climate Dyn*. 47:3335–57
109. Francey RJ, Tans PP. 1987. Latitudinal variation in oxygen-18 of atmospheric CO_2. *Nature* 327:495–97
110. Brenninkmeijer CAM, Kraft P, Mook WG. 1983. Oxygen isotope fractionation between CO_2 and H_2O. *Chem. Geol.* 41:181–90
111. Rozanski K, Araguás-Araguás L, Gonfiantini R. 1993. Isotopic patterns in modern global precipitation. In *Climate Change in Continental Isotopic Records*, Vol. 78, ed. PK Swart, KC Lohmann, J Mckenzie, S Savin, pp. 1–36. Washington, DC: Am. Geophys. Union
112. Dongmann G, Nurnberg HW, Forstel H, Wagener K. 1974. Enrichment of $H_2{}^{18}O$ in leaves of transpiring plants. *Radiation Environ. Biophys.* 11:41–52
113. Keeling RF. 1995. The atmospheric oxygen cycle: the oxygen isotopes of atmospheric CO_2 and O_2 and the O_2/N_2 ratio. *Rev. Geophys.* 33:1253–62
114. Tans PP. 1998. Oxygen isotopic equilibrium between carbon dioxide and water in soils. *Tellus B*. 50:163–78
115. Gillon J, Yakir D. 2001. Influence of carbonic anhydrase activity in terrestrial vegetation on the ^{18}O content of atmospheric CO_2. *Science* 291:2584–87
116. Wingate L, Ogee J, Cuntz M, Genty B, Reiter I, et al. 2009. The impact of soil microorganisms on the global budget of $\delta^{18}O$ in atmospheric CO_2. *PNAS* 106:22411–15
117. Welp LR, Keeling RF, Meijer HAJ, Bollenbacher AF, Piper SC, et al. 2011. Interannual variability in the oxygen isotopes of atmospheric CO_2 driven by El Niño. *Nature* 477:579–82
118. Liang M-C, Mahata S, Laskar AH, Thiemens MH, Newman S. 2017. Oxygen isotope anomaly in tropospheric CO_2 and implications for CO_2 residence time in the atmosphere and gross primary productivity. *Sci. Rep.* 7:13180
119. Berry J, Wolf A, Campbell JE, Baker I, Blake N, et al. 2013. A coupled model of the global cycles of carbonyl sulfide and CO_2: a possible new window on the carbon cycle. *J. Geophys. Res. Biogeosci.* 118:842–52
120. Campbell J, Carmichael G, Chai T, Mena-Carrasco M, Tang Y, et al. 2008. Photosynthetic control of atmospheric carbonyl sulfide during the growing season. *Science* 322:1085–88
121. Stimler K, Berry JA, Montzka SA, Yakir D. 2011. Association between carbonyl sulfide uptake and $^{18}\Delta$ during gas exchange in C_3 and C_4 leaves. *Plant Physiol.* 157:509–17
122. Aydin M, Britten GL, Montzka SA, Buizert C, Primeau F, et al. 2020. Anthropogenic impacts on atmospheric carbonyl sulfide since the 19th century inferred from polar firn air and ice core measurements. *J. Geophys. Res. Atmos.* 125:e2020JD033074
123. Brühl C, Lelieveld J, Crutzen P, Tost H, Stier P. 2012. The role of carbonyl sulphide as a source of stratospheric sulphate aerosol and its impact on climate. *Atmos. Chem. Phys.* 12:1239–53

124. Montzka SA, Calvert P, Hall BD, Elkins JW, Conway TJ, et al. 2007. On the global distribution, seasonality, and budget of atmospheric carbonyl sulfide (COS) and some similarities to CO_2. *J. Geophys. Res. Atmos.* 112:D09302
125. Cuntz M, Ciais P, Hoffmann G, Allison CE, Francey RJ, et al. 2003. A comprehensive global three-dimensional model of $\delta^{18}O$ in atmospheric CO_2: 2. Mapping the atmospheric signal. *J. Geophys. Res. Atmos.* 108:4528
126. Campbell J, Berry J, Seibt U, Smith S, Montzka S, et al. 2017. Large historical growth in global terrestrial gross primary production. *Nature* 544:84–87
127. Manning AC, Keeling RF. 2006. Global oceanic and land biotic carbon sinks from the Scripps atmospheric oxygen flask sampling network. *Tellus B.* 58:95–116
128. Woodwell GM, Whittaker RH, Reiners WA, Likens GE, Delwiche CC, Botkin DB. 1978. Biota and world carbon budget. *Science* 199:141–46
129. Bolin B, Eriksson E. 1959. Changes in the carbon dioxide content of the atmosphere and sea due to fossil fuel combustion. In *Rossby Memorial Volume*, ed. B Bolin, pp. 130–42. New York: Rockefeller Inst. Press, Oxford Univ. Press
130. Gruber N. 2011. Warming up, turning sour, losing breath: ocean biogeochemistry under global change. *Philos. Trans. R. Soc. A.* 369:1980–96
131. Landschützer P, Gruber N, Bakker D, Schuster U. 2014. Recent variability of the global ocean carbon sink. *Glob. Biogeochem. Cycle* 28:927–49
132. Le Quéré C, Rodenbeck C, Buitenhuis ET, Conway TJ, Langenfelds R, et al. 2007. Saturation of the Southern Ocean CO_2 sink due to recent climate change. *Science* 316:1735–38
133. Jones C, Robertson E, Arora V, Friedlingstein P, Shevliakova E, et al. 2013. Twenty-first-century compatible CO_2 emissions and airborne fraction simulated by CMIP5 earth system models under four representative concentration pathways. *J. Climate* 26:4398–413
134. Jones CD, Ciais P, Davis SJ, Friedlingstein P, Gasser T, et al. 2016. Simulating the Earth system response to negative emissions. *Environ. Res. Lett.* 11:095012
135. Wang X, Piao S, Ciais P, Friedlingstein P, Myneni RB, et al. 2014. A two-fold increase of carbon cycle sensitivity to tropical temperature variations. *Nature* 506:212–15
136. Lan X, Tans P, Sweeney C, Andrews A, Jacobson A, et al. 2017. Gradients of column CO_2 across North America from the NOAA Global Greenhouse Gas Reference Network. *Atmos. Chem. Phys.* 17:15151–65
137. Crisp D, Atlas RM, Breon F-M, Brown LR, Burrows JP, et al. 2004. The orbiting carbon observatory (OCO) mission. *Adv. Space Res.* 34:700–9
138. Wunch D, Wennberg P, Messerschmidt J, Parazoo N, Toon G, et al. 2013. The covariation of Northern Hemisphere summertime CO_2 with surface temperature in boreal regions. *Atmos. Chem. Phys.* 13:9447–59
139. Scholze M, Buchwitz M, Dorigo W, Guanter L, Quegan S. 2017. Reviews and syntheses: systematic Earth observations for use in terrestrial carbon cycle data assimilation systems. *Biogeosciences* 14:3401–29
140. van der Laan-Luijkx IT, van der Velde IR, van der Veen E, Tsuruta A, Stanislawska K, et al. 2017. The CarbonTracker Data Assimilation Shell (CTDAS) v1.0: implementation and global carbon balance 2001–2015. *Geosci. Model Dev.* 10:2785–800
141. van der Velde IR, Miller JB, van der Molen MK, Tans PP, Vaughn BH, et al. 2018. The CarbonTracker Data Assimilation System for CO_2 and $\delta^{13}C$ (CTDAS-C13 v1. 0): retrieving information on land-atmosphere exchange processes. *Geosci. Model Dev.* 11:283–304
142. Affek H, Yakir D. 2014. The stable isotopic composition of atmospheric CO_2. In *Treatise on Geochemistry*, Vol. 5: *The Atmosphere*, ed. RF Keeling, L Russell, pp. 179–212. Amsterdam: Elsevier. 2nd ed.
143. Friedlingstein P, Prentice IC. 2010. Carbon–climate feedbacks: a review of model and observation based estimates. *Curr. Opin. Environ. Sustain.* 2:251–57